Advanced models for smart multilayered plates based on Reissner Mixed Variational Theorem

I. Benedetti, A. Milazzo*

Dipartimento di Ingegneria Civile, Ambientale, Aerospaziale, dei Materiali - DICAM
Università degli Studi di Palermo, Viale delle Scienze, 90128, Palermo, Italy

Abstract

In the present work, families of equivalent singe layer and layer-wise models for the static and free vibrations analysis of magneto-electro-elastic multilayered plates are developed. The models are defined in the framework of a unified formulation, which offers a systematic approach for generating refined plate theories through suitable expansions of the through-the-thickness components of the relevant fields, considering the expansion order as a free parameter. The key features of the developed formulation are: *a*) the condensation of the electric and magnetic description into the mechanical representation, based on the quasi-static electric-magnetic approximation, which allows to reduce the computation of the analysis for both layer-wise and equivalent single layer models; *b*) the employment of the Reissner Mixed Variational Theorem, in which the displacements and transverse stress components are used as primary variables, thus allowing the explicit fulfilment of the transverse stress interface equilibrium. The proposed methodology is assessed by generating different layer-wise and equivalent single layer models for the analysis of thick magneto-electro-elastic layer and comparing their solution against available three-dimensional analytic results.

Keywords: smart plates, magneto-electro-elastic materials, advanced plate theories

*Corresponding author
Email addresses: ivano.benedetti@unipa.it (I. Benedetti), alberto.milazzo@unipa.it (A. Milazzo)

1. Introduction

Multi-physics materials, such as piezo-electric (PZ) or magneto-electro-elastic (MEE) materials, are today largely employed in several scientific and technological applications, as the coupling between different fields, e.g. mechanical, electric, magnetic, can be advantageously used for different purposes, such as structural health monitoring (SHM), vibration control, structural morphing, energy harvesting [1]. In aerospace and mechanical engineering applications, the employment of piezo-electric or MEE materials has led to the concept of smart structure, in which the structural components are endowed with multifunctional sensing or acting capabilities. In this framework, the use of piezoelectric materials is today prevalent, while MEE materials are emerging as an interesting alternative with extended functionalities, due to the possibility of exploiting the additional coupling with the magnetic field [2]. Among the different possible applications, much research has been focused on the development of composite laminates with embedded multi-functional layers, often referred to as *smart laminates* [3–5].

One of the factors supporting the successful design of smart structural systems is the availability of reliable modelling tools, essential for supporting experimental testing and reducing its cost. In the case of piezoelectric or MEE materials, the models must accurately represent the complex interactions among the different fields. Several analytical, numerical and computational techniques have been developed for the study of systems involving attached or embedded piezoelectric and MEE elements [6–19]). The present work focuses of the modelling of smart composite plates with general lay-ups of MEE layers.

Several two-dimensional (2D) laminate plate theories have been developed, with the aim of enabling suitable accuracy at affordable computational cost: both layer-wise (LW) [20, 21] and equivalent-single layer (ESL) [22, 23] approaches have been proposed in the literature. LW techniques offer high accuracy, but their computational cost increases with the number of layers. On the other

hand, the computational cost of ESL models is independent from the number of layers, thus resulting in more affordable computations; however, their accuracy is generally reduced with respect to that obtained through LW approaches, especially for thick laminates, whose reliable analysis generally requires higher order theories.

Both LW and ESL theories for smart plates have been generally formulated using the electric and magnetic primary quantities as independent state variables of the problem, see Ref. [24] and references therein; recently, models for smart MEE laminates have been developed employing the concept of effective plate, resulting from the condensation of the electric and magnetic state into the mechanical variables [25–27]. Such theories are usually based on generalised variational statements extending the application of the variational theorems of classical elasticity [28, 29]. Most of the proposed models are based on the extension of the principle of virtual displacements (PVD), where the generalised displacement components are seen as primary variables and the in-plane stress components are calculated using Hooke's law. While these theories might produce accurate predictions for the displacement and in-plane stress components, they might fail to yield the same accuracy for the transverse shear and normal stresses. To overcome this drawback, the Reissner mixed variational theorem (RMVT) can be invoked [30, 31], where the displacement and transverse stress components are employed as primary variables and the in-plane stress components are derived from these.

Starting from the PVD and RMVT for the formulation and implementation of both LW and ESL refined higher order theories for multilayered plates, Carrera proposed a powerful approach known as Carrera Unified Formulation (CUF), whose underlying ideas, principles and implementation issues for mechanical problems is reviewed in Refs. [32] and [33]. The CUF offers a systematic methodology for generating refined plate models, considering the order of the theory as a free parameter of the formulation. The CUF has been used for smart laminates with both piezoelectric, see Ref. [24] and references therein, and MEE layers [34–36] .

By using the unified formulation and the generalised PVD for smart materials, Milazzo and co-workers presented families of ESL and LW models for MEE multilayered plates involving only mechanical kinematical variables, as the electric and magnetic state is preliminarily condensed into the mechanical description [37, 38]. The formulation has been extended to geometric non-linearities [39] and finite elements have been formulated based on the proposed models [40]. Starting from the sketched context, in the present work, families of ESL and LW models for MEE multilayered plates, with the condensation of the electric and magnetic fields into the mechanical description, are developed. The novelty of the formulation consists in the use of the generalised RMVT variational statement in the framework of the CUF, which enhances the model reliability through the fulfilment of transverse stress interface continuity.

2. Basic equations

Let us consider a multilayered plate comprising N homogeneous orthotropic MEE layers, all with poling direction along the plate thickness. The plate is referred to a three-dimensional coordinate system, with the x_1 and x_2 axes lying on the plate mid-plane Ω, bounded by the curve $\partial\Omega$, and the x_3 axis directed along the plate thickness (see Fig. 1).

In the following, we will refer to vector and tensor components directed along x_1 and x_2 as in-plane components and to x_3 components as out-of-plane components. The plate may be generally subjected to mechanical loads and to electric and magnetic actions applied on the top and bottom surfaces.

2.1. Gradient equations

The mechanical gradient equations, namely the strain-displacement relations, are

$$\boldsymbol{\varepsilon} = \boldsymbol{\mathcal{D}}_p \boldsymbol{u}, \qquad \boldsymbol{\gamma} = \boldsymbol{\mathcal{D}}_n \boldsymbol{u} + \boldsymbol{\mathcal{D}}_{x_3} \boldsymbol{u} \tag{1}$$

where $\boldsymbol{u}^T = \left\{ u_1 \;\; u_2 \;\; u_3 \right\}$ is the displacement vector and $\boldsymbol{\varepsilon}^T = \left\{ \varepsilon_{11} \;\; \varepsilon_{22} \;\; \varepsilon_{12} \right\}$ and $\boldsymbol{\gamma}^T = \left\{ \varepsilon_{31} \;\; \varepsilon_{32} \;\; \varepsilon_{33} \right\}$ are the vectors collecting the in-plane and out-of-plane components of the strain field, respectively.

The differential operators appearing in Eq. (1) are defined as

$$\boldsymbol{\mathcal{D}}_p = \begin{bmatrix} \partial_1 & 0 & 0 \\ 0 & \partial_2 & 0 \\ \partial_2 & \partial_1 & 0 \end{bmatrix}, \qquad \boldsymbol{\mathcal{D}}_n = \begin{bmatrix} 0 & 0 & \partial_1 \\ 0 & 0 & \partial_2 \\ 0 & 0 & 0 \end{bmatrix}, \qquad \boldsymbol{\mathcal{D}}_{x_3} = \begin{bmatrix} \partial_3 & 0 & 0 \\ 0 & \partial_3 & 0 \\ 0 & 0 & \partial_3 \end{bmatrix} = \boldsymbol{\mathcal{D}}_i \partial_3 \tag{2}$$

where $\partial_i = \partial(\cdot)/\partial x_i$ and $\boldsymbol{\mathcal{D}}_i$ is the 3×3 identity matrix.

As the elastic waves propagate several order of magnitude slower than the electromagnetic ones, the approximation of quasi-static electro-magnetic behaviour is assumed: introducing the electric potential Φ and the magnetic scalar potential Ψ, the electric and magnetic gradient equations are written as

$$\boldsymbol{E}_p = -\boldsymbol{\nabla}_p \Phi, \qquad \boldsymbol{E}_n = -\boldsymbol{\nabla}_n \Phi, \tag{3}$$

$$\boldsymbol{H}_p = -\boldsymbol{\nabla}_p \Psi, \qquad \boldsymbol{H}_n = -\boldsymbol{\nabla}_n \Psi, \tag{4}$$

where $\boldsymbol{E}_p^T = \left\{ E_1 \;\; E_2 \right\}$ and $\boldsymbol{H}_p^T = \left\{ H_1 \;\; H_2 \right\}$ are the vector collecting the in-plane components of the electric field $\boldsymbol{E}$ and the magnetic field $\boldsymbol{H}$, $\boldsymbol{E}_n^T = \left\{ E_3 \right\}$ and $\boldsymbol{H}_n^T = \left\{ H_3 \right\}$ are the vectors of the corresponding out-of-plane components and

$$\boldsymbol{\nabla}_p = \begin{bmatrix} \partial_1 & \partial_2 \end{bmatrix}^T, \qquad \boldsymbol{\nabla}_n = \begin{bmatrix} \partial_3 \end{bmatrix}. \tag{5}$$

2.2. Constitutive equations

The constitutive law for an orthotropic MEE composite with electric and magnetic poling directions parallel to the x_3-axis is compactly written as

$$\begin{Bmatrix} \boldsymbol{\sigma} \\ \boldsymbol{\tau} \\ \boldsymbol{D}_p \\ \boldsymbol{D}_n \\ \boldsymbol{B}_p \\ \boldsymbol{B}_n \end{Bmatrix} = \begin{bmatrix} \boldsymbol{C}_{pp} & \boldsymbol{C}_{pn} & \mathbf{0} & -\boldsymbol{e}_{np}{}^T & \mathbf{0} & -\boldsymbol{q}_{np}{}^T \\ \boldsymbol{C}_{np} & \boldsymbol{C}_{nn} & -\boldsymbol{e}_{pn}{}^T & -\boldsymbol{e}_{nn}{}^T & -\boldsymbol{q}_{pn}{}^T & -\boldsymbol{q}_{nn}{}^T \\ \mathbf{0} & \boldsymbol{e}_{pn} & \boldsymbol{\epsilon}_{pp} & \mathbf{0} & \boldsymbol{d}_{pp} & \mathbf{0} \\ \boldsymbol{e}_{np} & \boldsymbol{e}_{nn} & \mathbf{0} & \boldsymbol{\epsilon}_{nn} & \mathbf{0} & \boldsymbol{d}_{nn} \\ \mathbf{0} & \boldsymbol{q}_{pn} & \boldsymbol{d}_{pp} & \mathbf{0} & \boldsymbol{\mu}_{pp} & \mathbf{0} \\ \boldsymbol{q}_{np} & \boldsymbol{q}_{nn} & \mathbf{0} & \boldsymbol{d}_{nn} & \mathbf{0} & \boldsymbol{\mu}_{nn} \end{bmatrix} \begin{Bmatrix} \boldsymbol{\varepsilon} \\ \boldsymbol{\gamma} \\ \boldsymbol{E}_p \\ \boldsymbol{E}_n \\ \boldsymbol{H}_p \\ \boldsymbol{H}_n \end{Bmatrix} \tag{6}$$

where $\boldsymbol{C}_{ij}$ are matrix blocks containing the elastic stiffness coefficients, the $\boldsymbol{\epsilon_{ij}}$ and $\boldsymbol{\mu_{ij}}$ blocks collect the dielectric constants and magnetic permeabilities respectively, whereas $\boldsymbol{e}_{ij}$, $\boldsymbol{q}_{ij}$ and $\boldsymbol{d}_{ij}$ collect the piezo-electric, piezo-magnetic and magneto-electric coupling coefficients. Consistently: $\boldsymbol{\sigma}^T = \left\{\sigma_{11} \;\; \sigma_{22} \;\; \sigma_{21}\right\}$ and $\boldsymbol{\tau}^T = \left\{\sigma_{31} \;\; \sigma_{32} \;\; \sigma_{33}\right\}$ are vectors collecting the in-plane and out-of-plane components of stress respectively; $\boldsymbol{D}_p^T = \left\{D_1 \;\; D_2\right\}$ and $\boldsymbol{D}_n^T = \left\{D_3\right\}$ collect the in-plane and out-of-plane components of the electric displacements; $\boldsymbol{B}_p^T = \left\{B_1 \;\; B_2\right\}$ and $\boldsymbol{B}_n^T = \left\{B_3\right\}$ collect the in-plane and out-of-plane components of the magnetic induction vector. It is worth noting that, for multilayered plates, the constitutive matrices depend on the x_3 coordinate. In the present work, they are considered constant within each laminate layer. For the application of variational theorems to the MEE problem, mixed forms of the constitutive equation are often invoked [41, 42]; in the present formulation, employing the extension of the Reissner Mixed Variational Theorem (RMVT) [30, 31], the

following mixed form is used

$$\begin{Bmatrix} \boldsymbol{\sigma} \\ \boldsymbol{\gamma} \\ \boldsymbol{D}_p \\ \boldsymbol{D}_n \\ \boldsymbol{B}_p \\ \boldsymbol{B}_n \end{Bmatrix} = \begin{bmatrix} \boldsymbol{C}_{\sigma\varepsilon} & \boldsymbol{C}_{\sigma\tau} & \boldsymbol{0} & \boldsymbol{C}_{\sigma E_n} & \boldsymbol{0} & \boldsymbol{C}_{\sigma H_n} \\ \boldsymbol{C}_{\gamma\varepsilon} & \boldsymbol{C}_{\gamma\tau} & \boldsymbol{C}_{\gamma E_p} & \boldsymbol{C}_{\gamma_n E_n} & \boldsymbol{C}_{\gamma_n H_p} & \boldsymbol{C}_{\gamma_n H_n} \\ \boldsymbol{0} & \boldsymbol{C}_{D_p\tau} & \boldsymbol{C}_{D_p E_p} & \boldsymbol{0} & \boldsymbol{C}_{D_p H_p} & \boldsymbol{0} \\ \boldsymbol{C}_{D_n\varepsilon} & \boldsymbol{C}_{D_n\tau} & \boldsymbol{0} & \boldsymbol{C}_{D_n E_n} & \boldsymbol{0} & \boldsymbol{C}_{D_n H_n} \\ \boldsymbol{0} & \boldsymbol{C}_{B_p\tau} & \boldsymbol{C}_{B_p E_p} & \boldsymbol{0} & \boldsymbol{C}_{B_p H_p} & \boldsymbol{0} \\ \boldsymbol{C}_{B_n\varepsilon} & \boldsymbol{C}_{B_n\tau} & \boldsymbol{0} & \boldsymbol{C}_{B_n E_n} & \boldsymbol{0} & \boldsymbol{C}_{B_n H_n} \end{bmatrix} \begin{Bmatrix} \boldsymbol{\varepsilon} \\ \boldsymbol{\tau} \\ \boldsymbol{E}_p \\ \boldsymbol{E}_n \\ \boldsymbol{H}_p \\ \boldsymbol{H}_n \end{Bmatrix}, \tag{7}$$

where the involved matrices have the form given in Appendix A.

2.3. Governing equations

The governing equations for a MEE body with volume V bounded by the frontier ∂V are obtained by generalising the Reissner Mixed Variational Principle (RMTV). Assuming that the gradient and constitutive equations are satisfied, it states that the solution of the MEE problem is given in terms of the displacement field $\boldsymbol{u}$, the out-of-plane stress field $\boldsymbol{\tau}$, the electric potential Φ and the magnetic potential Ψ, i.e. the primary variables, which make stationary the functional

$$\begin{aligned} \Pi = & \int_V \left(\boldsymbol{\varepsilon}^T \boldsymbol{\sigma} + \boldsymbol{\tau}^T \boldsymbol{\gamma} - \boldsymbol{E}_p^T \boldsymbol{D}_p - \boldsymbol{E}_n^T \boldsymbol{D}_n - \boldsymbol{H}_p^T \boldsymbol{B}_p - \boldsymbol{H}_n^T \boldsymbol{B}_n \right) dV + \\ & + \int_V \boldsymbol{\tau}^T \left(\boldsymbol{\gamma} - \hat{\boldsymbol{\gamma}} \right) dV - \int_V \rho \boldsymbol{u}^T \ddot{\boldsymbol{u}} \, dV + \\ & - \int_V \left(\boldsymbol{u}^T \bar{\boldsymbol{f}} - \Phi \bar{q} \right) dV - \int_{\partial V} \left(\boldsymbol{u}^T \bar{\boldsymbol{t}} - \Phi \bar{Q} \right) d\partial V \end{aligned} \tag{8}$$

where $\bar{\boldsymbol{t}}$ are the applied surface tractions, $\bar{\boldsymbol{f}}$ are body forces, ρ is the mass density, $\bar{Q}$ and $\bar{q}$ are the surface and body free electric charge densities and the overdot denotes the derivative with respect to the time t. In Eq. (8) the superimposed hat denotes quantities evaluated via the constitutive equations whereas the other quantities depending on the primary variables are evaluated via the gradient equations. Taking the first variation of Eq. (8) and integrating by parts, through standard calculus of variations, one obtains:

i) The equilibrium equations and the Gauss' laws for electro-statics and magneto-statics, holding in the volume V

$$\delta \boldsymbol{u}: \qquad \boldsymbol{\mathcal{D}}_p^T \boldsymbol{\sigma} + \boldsymbol{\mathcal{D}}_n^T \boldsymbol{\tau} + \boldsymbol{\mathcal{D}}_{x_3}^T \boldsymbol{\tau} + \bar{\boldsymbol{f}} - \rho \ddot{\boldsymbol{u}} = \boldsymbol{0} \tag{9a}$$

$$\delta \Phi: \qquad \boldsymbol{\nabla}_p^T \boldsymbol{D}_p + \boldsymbol{\nabla}_n \boldsymbol{D}_n + \bar{q} = 0 \tag{9b}$$

$$\delta \Psi: \qquad \boldsymbol{\nabla}_p^T \boldsymbol{B}_p + \boldsymbol{\nabla}_n \boldsymbol{B}_n = 0 \tag{9c}$$

(the conjugated varied fields are indicated for the sake of completeness).

ii) The compatibility equation for the out-of-plane strains holding in the volume V

$$\delta \boldsymbol{\tau}: \qquad \boldsymbol{\gamma} - \hat{\boldsymbol{\gamma}} = \boldsymbol{0} \tag{10}$$

iii) The natural boundary conditions holding on the boundary ∂V

$$\delta \boldsymbol{u}: \qquad \widetilde{\boldsymbol{\mathcal{D}}}_p^T \boldsymbol{\sigma} + \widetilde{\boldsymbol{\mathcal{D}}}_n^T \boldsymbol{\tau} + \widetilde{\boldsymbol{\mathcal{D}}}_{x_3}^T \boldsymbol{\tau} = \bar{\boldsymbol{t}} \tag{11a}$$

$$\delta \Phi: \qquad \widetilde{\boldsymbol{\nabla}}_p^T \boldsymbol{D}_p + \widetilde{\boldsymbol{\nabla}}_n \boldsymbol{D}_n = \bar{Q} \tag{11b}$$

$$\delta \Psi: \qquad \widetilde{\boldsymbol{\nabla}}_p^T \boldsymbol{B}_p + \widetilde{\boldsymbol{\nabla}}_n \boldsymbol{B}_n = 0 \tag{11c}$$

In Eqs.(11) the boundary operators $\widetilde{\boldsymbol{\mathcal{D}}}_{(\cdot)}$ and $\widetilde{\boldsymbol{\nabla}}_{(\cdot)}$ are obtained from the differential operators $\boldsymbol{\mathcal{D}}_{(\cdot)}$ and $\boldsymbol{\nabla}_{(\cdot)}$ by substituting the partial derivatives $\partial_i = \partial(\cdot)/\partial x_i$ with the corresponding boundary outward direction cosines n_i.

3. Formulation

To develop the advanced refined theories for multilayered smart plates proposed in the present paper, extensive use of the indicial notation is adopted, according to the following specifications. A superscript $\langle k \rangle$ is used to denote quantities associated with the k-th layer of the laminate. Unless otherwise specified, it is assumed that $\alpha, \beta \in \{0, 1, \ldots, M_u\}$ where $M_u + 1$ is the number of terms of the displacement expansion, $\lambda, \mu \in \{0, 1, \ldots, M_\tau\}$ where $M_\tau + 1$ is the

number of terms of the transverse stress expansion, $k, i \in \{1, 2, \ldots, N\}$ where N is the number of layers in the laminate. Finally, the notation $\sum_{r,s} = \sum_{r} \sum_{s}$ is used to indicate multiple summation with respect to the indexes r and s raging over the associated standard set.

3.1. Mechanical variables modeling

Within each layer k of the laminate, the displacement field and the out-of-plane stresses are modelled as an expansion along the plate thickness of so-called *thickness functions* $F_\alpha\left(x_3\right)$ and $\tilde{F}_\alpha\left(x_3\right)$, respectively [32, 33]. One writes

$$\boldsymbol{u}^{\langle k \rangle}(x_1, x_2, x_3) = \sum_{\alpha=0}^{M_u} \boldsymbol{u}_\alpha^{\langle k \rangle}(x_1, x_2) F_\alpha^{\langle k \rangle}(x_3) = \sum_{\alpha} F_\alpha^{\langle k \rangle} \boldsymbol{u}_\alpha^{\langle k \rangle} \tag{12a}$$

$$\boldsymbol{\tau}^{\langle k \rangle}(x_1, x_2, x_3) = \sum_{\lambda=0}^{M_\tau} \boldsymbol{\tau}_\lambda^{\langle k \rangle}(x_1, x_2) \tilde{F}_\lambda^{\langle k \rangle}(x_3) = \sum_{\lambda} \tilde{F}_\lambda^{\langle k \rangle} \boldsymbol{\tau}_\lambda^{\langle k \rangle} \tag{12b}$$

Using the gradient relationships, Eqs.(1), the corresponding mechanical strain field is written as

$$\boldsymbol{\varepsilon}^{\langle k \rangle} = \sum_{\alpha} F_\alpha^{\langle k \rangle} \boldsymbol{\mathcal{D}}_p \boldsymbol{u}_\alpha^{\langle k \rangle} \tag{13a}$$

$$\boldsymbol{\gamma}^{\langle k \rangle} = \sum_{\alpha} \left(F_\alpha^{\langle k \rangle} \boldsymbol{\mathcal{D}}_n + \frac{\partial F_\alpha^{\langle k \rangle}}{\partial x_3} \boldsymbol{\mathcal{D}}_i \right) \boldsymbol{u}_\alpha^{\langle k \rangle} \tag{13b}$$

3.2. Electro-magnetic variables modeling

The two-dimensional nature of plates allows simplifying assumptions on the electromagnetic behaviour of smart plates [37]. For both thin and thick plates, the in-plane derivatives of the in-plane components of the electric displacement and magnetic induction can be assumed negligible with respect to the out-of-plane components. Thus in particular it holds $\partial D_j / \partial x_j = \partial B_j / \partial x_j = 0$ for $j = 1, 2$ and using Eqs.(7), (1), (3) and (4) into the Gauss' equations for electrostatics and magnetostatics, namely Eqs. (9b) and (9c), one infers the

following system of equations holding for each k-th layer

$$\begin{cases} \boldsymbol{C}^{\langle k\rangle}_{D_n E_n}\dfrac{\partial^2\Phi^{\langle k\rangle}}{\partial x_3^2}+\boldsymbol{C}^{\langle k\rangle}_{D_n H_n}\dfrac{\partial^2\Psi^{\langle k\rangle}}{\partial x_3^2}=\boldsymbol{C}^{\langle k\rangle}_{D_n \varepsilon}\dfrac{\partial\boldsymbol{\varepsilon}^{\langle k\rangle}}{\partial x_3}+\boldsymbol{C}^{\langle k\rangle}_{D_n \tau}\dfrac{\partial\boldsymbol{\tau}^{\langle k\rangle}}{\partial x_3} \\ \boldsymbol{C}_{B_n E_n}\dfrac{\partial^2\Phi^{\langle k\rangle}}{\partial x_3^2}+\boldsymbol{C}_{B_n H_n}\dfrac{\partial^2\Psi^{\langle k\rangle}}{\partial x_3^2}=\boldsymbol{C}_{B_n \varepsilon}\dfrac{\partial\boldsymbol{\varepsilon}^{\langle k\rangle}}{\partial x_3}+\boldsymbol{C}_{B_n \tau}\dfrac{\partial\boldsymbol{\tau}^{\langle k\rangle}}{\partial x_3} \end{cases} \tag{14}$$

Taking the mechanical variable approximation into account, namely Eqs. (12b) and (13a), one obtains

$$\frac{\partial^2\Phi^{\langle k\rangle}}{\partial x_3^2}=\sum_\alpha\frac{\partial F^{\langle k\rangle}_\alpha}{\partial x_3}\boldsymbol{\mathcal{A}}^{\langle k\rangle}_{\Phi\varepsilon}\boldsymbol{\mathcal{D}}_p\boldsymbol{u}^{\langle k\rangle}_\alpha+\sum_\lambda\frac{\partial\tilde{F}^{\langle k\rangle}_\lambda}{\partial x_3}\boldsymbol{\mathcal{A}}^{\langle k\rangle}_{\Phi\tau}\boldsymbol{\tau}^{\langle k\rangle}_\lambda \tag{15a}$$

$$\frac{\partial^2\Psi^{\langle k\rangle}}{\partial x_3^2}=\sum_\alpha\frac{\partial F^{\langle k\rangle}_\alpha}{\partial x_3}\boldsymbol{\mathcal{A}}^{\langle k\rangle}_{\Psi\varepsilon}\boldsymbol{\mathcal{D}}_p\boldsymbol{u}^{\langle k\rangle}_\alpha+\sum_\lambda\frac{\partial\tilde{F}^{\langle k\rangle}_\lambda}{\partial x_3}\boldsymbol{\mathcal{A}}^{\langle k\rangle}_{\Psi\tau}\boldsymbol{\tau}^{\langle k\rangle}_\lambda \tag{15b}$$

where for $r\in\{\varepsilon,\tau\}$

$$\begin{bmatrix}\boldsymbol{\mathcal{A}}^{\langle k\rangle}_{\Phi r}\\ \boldsymbol{\mathcal{A}}^{\langle k\rangle}_{\Psi r}\end{bmatrix}=\begin{bmatrix}\boldsymbol{C}^{\langle k\rangle}_{D_n E_n} & \boldsymbol{C}^{\langle k\rangle}_{D_n H_n}\\ \boldsymbol{C}^{\langle k\rangle}_{B_n E_n} & \boldsymbol{C}^{\langle k\rangle}_{B_n H_n}\end{bmatrix}^{-1}\begin{bmatrix}\boldsymbol{C}^{\langle k\rangle}_{D_n r}\\ \boldsymbol{C}^{\langle k\rangle}_{B_n r}\end{bmatrix} \tag{16}$$

Integrating twice Eqs.(15) gives

$$\Phi^{\langle k\rangle}=\sum_\alpha G^{\langle k\rangle}_\alpha\boldsymbol{\mathcal{A}}^{\langle k\rangle}_{\Phi\varepsilon}\boldsymbol{\mathcal{D}}_p\boldsymbol{u}^{\langle k\rangle}_\alpha+\sum_\lambda\tilde{G}^{\langle k\rangle}_\lambda\boldsymbol{\mathcal{A}}^{\langle k\rangle}_{\Phi\tau}\boldsymbol{\tau}^{\langle k\rangle}_\lambda+x_3a^{\langle k\rangle}_\Phi+b^{\langle k\rangle}_\Phi \tag{17a}$$

$$\Psi^{\langle k\rangle}=\sum_\alpha G^{\langle k\rangle}_\alpha\boldsymbol{\mathcal{A}}^{\langle k\rangle}_{\Psi\varepsilon}\boldsymbol{\mathcal{D}}_p\boldsymbol{u}^{\langle k\rangle}_\alpha+\sum_\lambda\tilde{G}^{\langle k\rangle}_\lambda\boldsymbol{\mathcal{A}}^{\langle k\rangle}_{\Psi\tau}\boldsymbol{\tau}^{\langle k\rangle}_\lambda+x_3a^{\langle k\rangle}_\Psi+b^{\langle k\rangle}_\Psi \tag{17b}$$

where $G^{\langle k\rangle}_\alpha(z)=\displaystyle\int F^{\langle k\rangle}_\alpha(z)dz$ and $\tilde{G}^{\langle k\rangle}_\lambda(z)=\displaystyle\int\tilde{F}^{\langle k\rangle}_\lambda(z)dz$. The integration constants $a^{\langle k\rangle}_\Phi$, $b^{\langle k\rangle}_\Phi$, $a^{\langle k\rangle}_\Psi$, and $b^{\langle k\rangle}_\Psi$ are determined by enforcing the electric and magnetic continuity conditions at the $N-1$ layers interfaces and external electric and magnetic boundary conditions at the top and bottom faces of the laminate. The electric and magnetic interface conditions are given by the continuity of the electric and magnetic potentials, normal electric displacement and magnetic induction; the electric and magnetic boundary conditions at the upper

and bottom laminate surfaces consist of prescribed potentials or normal electric displacement and magnetic induction, whose values are collected in the vector $\boldsymbol{\xi}$. According with the form of enforced electric and magnetic interface and boundary conditions, a system of equations of the form

$$\boldsymbol{\mathscr{A}}\boldsymbol{x} = \sum_{i,\alpha} \boldsymbol{\mathscr{B}}_{i\alpha} \boldsymbol{\mathcal{D}}_p \boldsymbol{u}_\alpha^{\langle i \rangle} + \sum_{i,\lambda} \boldsymbol{\mathscr{C}}_{i\lambda} \boldsymbol{\tau}_\lambda^{\langle i \rangle} + \boldsymbol{\mathscr{W}}\boldsymbol{\xi} \tag{18}$$

is obtained, where $\boldsymbol{x}$ is a vector collecting the layers integration constants and $\boldsymbol{\mathscr{A}}$, $\boldsymbol{\mathscr{B}}_{i\alpha}$, $\boldsymbol{\mathscr{C}}_{i\lambda}$ and $\boldsymbol{\mathscr{W}}$ are matrices involving the layers material properties and thickness functions only. Details on the procedure used to derive Eq.(18) are given in Ref.[38]; they are not reported in the present paper for the sake of conciseness. Therefore, the integration constants can be compactly written in the general form

$$z_\Lambda^{\langle k \rangle} = \sum_{i,\alpha} \boldsymbol{z}_{\Lambda_\varepsilon \alpha}^{\langle ki \rangle} \boldsymbol{\mathcal{D}}_p \boldsymbol{u}_\alpha^{\langle i \rangle} + \sum_{i,\lambda} \boldsymbol{z}_{\Lambda_\tau \lambda}^{\langle ki \rangle} \boldsymbol{\tau}_\lambda^{\langle i \rangle} + \boldsymbol{z}_{\Lambda\xi}^{\langle k \rangle} \boldsymbol{\xi} \tag{19}$$

where the symbol z stands for a or b and the symbol Λ stands for Φ or Ψ, so that Eq.(19) holds for $a_\Phi^{\langle k \rangle}$, $b_\Phi^{\langle k \rangle}$, $a_\Psi^{\langle k \rangle}$, and $b_\Psi^{\langle k \rangle}$. It is worth remarking that in Eq.(19) the (1×3) row arrays $\boldsymbol{z}_{\Lambda_\varepsilon \alpha}^{\langle ki \rangle}$ and $\boldsymbol{z}_{\Lambda_\tau \lambda}^{\langle ki \rangle}$ collect the coefficients expressing the effects on the k-th layer's potential Λ of the i-th layer strains terms $\boldsymbol{\mathcal{D}}_p \boldsymbol{u}_\alpha^{\langle i \rangle}$ and transverse stresses terms $\boldsymbol{\tau}_\alpha^{\langle i \rangle}$. Finally, the (1×4) row array $\boldsymbol{z}_{\Lambda\xi}$ collects the coefficients expressing the influence on the potential Λ of the electric and magnetic boundary conditions $\boldsymbol{\xi}$. In conclusion, the electric and magnetic state is described by the following expression of the potentials

$$\Phi^{\langle k \rangle} = \sum_{i,\alpha} \tilde{\boldsymbol{\mathscr{A}}}_{\Phi_\varepsilon \alpha}^{\langle ki \rangle} \boldsymbol{\mathcal{D}}_p \boldsymbol{u}_\alpha^{\langle i \rangle} + \sum_{i,\lambda} \tilde{\boldsymbol{\mathscr{A}}}_{\Phi_\tau \lambda}^{\langle ki \rangle} \boldsymbol{\tau}_\lambda^{\langle i \rangle} + \tilde{\boldsymbol{\mathscr{A}}}_{\Phi_\xi}^{\langle k \rangle} \boldsymbol{\xi} \tag{20a}$$

$$\Psi^{\langle k \rangle} = \sum_{i,\alpha} \tilde{\boldsymbol{\mathscr{A}}}_{\Psi_\varepsilon \alpha}^{\langle ki \rangle} \boldsymbol{\mathcal{D}}_p \boldsymbol{u}_\alpha^{\langle i \rangle} + \sum_{i,\lambda} \tilde{\boldsymbol{\mathscr{A}}}_{\Psi_\tau \lambda}^{\langle ki \rangle} \boldsymbol{\tau}_\lambda^{\langle i \rangle} + \tilde{\boldsymbol{\mathscr{A}}}_{\Psi_\xi}^{\langle k \rangle} \boldsymbol{\xi} \tag{20b}$$

where, for $\Lambda = \Phi, \Psi$, the following relations hold

$$\tilde{\boldsymbol{\mathcal{A}}}^{\langle ki\rangle}_{\Lambda_\varepsilon\alpha} = G_\alpha \boldsymbol{\mathcal{A}}^{\langle k\rangle}_{\Lambda\varepsilon}\delta_{ki} + x_3 \boldsymbol{a}^{\langle ki\rangle}_{\Lambda_\varepsilon\alpha} + \boldsymbol{b}^{\langle ki\rangle}_{\Lambda_\varepsilon\alpha} \tag{21}$$

$$\tilde{\boldsymbol{\mathcal{A}}}^{\langle ki\rangle}_{\Lambda_\tau\lambda} = \tilde{G}_\lambda \boldsymbol{\mathcal{A}}^{\langle k\rangle}_{\Lambda\tau}\delta_{ki} + x_3 \boldsymbol{a}^{\langle ki\rangle}_{\Lambda_\tau\lambda} + \boldsymbol{b}^{\langle ki\rangle}_{\Lambda_\tau\lambda} \tag{22}$$

$$\tilde{\boldsymbol{\mathcal{A}}}^{\langle k\rangle}_{\Lambda_\xi} = x_3 \boldsymbol{a}^{\langle k\rangle}_{\Lambda\xi} + \boldsymbol{b}^{\langle k\rangle}_{\Lambda\xi} \tag{23}$$

By using Eqs.(3) and (4), the expressions for the in- and out-of-plane components of the electric and magnetic fields are obtained as

$$\begin{aligned}\boldsymbol{E}_p = &-\sum_{i,\alpha}\left\{\boldsymbol{I}_1\tilde{\boldsymbol{\mathcal{A}}}^{\langle ki\rangle}_{\Phi_\varepsilon\alpha}\frac{\partial \boldsymbol{\mathcal{D}}_p \boldsymbol{u}^{\langle i\rangle}_\alpha}{\partial x_1} + \boldsymbol{I}_2\tilde{\boldsymbol{\mathcal{A}}}^{\langle ki\rangle}_{\Phi_\varepsilon\alpha}\frac{\partial \boldsymbol{\mathcal{D}}_p \boldsymbol{u}^{\langle i\rangle}_\alpha}{\partial x_2}\right\} - \\ &\sum_{i,\lambda}\left\{\boldsymbol{I}_1\tilde{\boldsymbol{\mathcal{A}}}^{\langle ki\rangle}_{\Phi_\tau\lambda}\frac{\partial \boldsymbol{\tau}^{\langle i\rangle}_\lambda}{\partial x_1} + \boldsymbol{I}_2\tilde{\boldsymbol{\mathcal{A}}}^{\langle ki\rangle}_{\Phi_\tau\lambda}\frac{\partial \boldsymbol{\tau}^{\langle i\rangle}_\lambda}{\partial x_2}\right\} - \boldsymbol{I}_1\tilde{\boldsymbol{\mathcal{A}}}^{\langle k\rangle}_{\Phi_\xi}\frac{\partial \boldsymbol{\xi}}{\partial x_1} - \boldsymbol{I}_2\tilde{\boldsymbol{\mathcal{A}}}^{\langle k\rangle}_{\Phi_\xi}\frac{\partial \boldsymbol{\xi}}{\partial x_2}\end{aligned} \tag{24a}$$

$$\boldsymbol{E}^{\langle k\rangle}_n = -\sum_{i,\alpha}\frac{\partial \tilde{\boldsymbol{\mathcal{A}}}^{\langle ki\rangle}_{\Phi_\varepsilon\alpha}}{\partial x_3}\boldsymbol{\mathcal{D}}_p \boldsymbol{u}^{\langle i\rangle}_\alpha - \sum_{i,\lambda}\frac{\partial \tilde{\boldsymbol{\mathcal{A}}}^{\langle ki\rangle}_{\Phi_\tau\lambda}}{\partial x_3}\boldsymbol{\tau}^{\langle i\rangle}_\lambda - \frac{\partial \tilde{\boldsymbol{\mathcal{A}}}^{\langle k\rangle}_{\Phi_\xi}}{\partial x_3}\boldsymbol{\xi} \tag{24b}$$

$$\begin{aligned}\boldsymbol{H}_p = &-\sum_{i,\alpha}\left\{\boldsymbol{I}_1\tilde{\boldsymbol{\mathcal{A}}}^{\langle ki\rangle}_{\Psi_\varepsilon\alpha}\frac{\partial \boldsymbol{\mathcal{D}}_p \boldsymbol{u}^{\langle i\rangle}_\alpha}{\partial x_1} + \boldsymbol{I}_2\tilde{\boldsymbol{\mathcal{A}}}^{\langle ki\rangle}_{\Psi_\varepsilon\alpha}\frac{\partial \boldsymbol{\mathcal{D}}_p \boldsymbol{u}^{\langle i\rangle}_\alpha}{\partial x_2}\right\} - \\ &\sum_{i,\lambda}\left\{\boldsymbol{I}_1\tilde{\boldsymbol{\mathcal{A}}}^{\langle ki\rangle}_{\Psi_\tau\lambda}\frac{\partial \boldsymbol{\tau}^{\langle i\rangle}_\lambda}{\partial x_1} + \boldsymbol{I}_2\tilde{\boldsymbol{\mathcal{A}}}^{\langle ki\rangle}_{\Psi_\tau\lambda}\frac{\partial \boldsymbol{\tau}^{\langle i\rangle}_\lambda}{\partial x_2}\right\} - \boldsymbol{I}_1\tilde{\boldsymbol{\mathcal{A}}}^{\langle k\rangle}_{\Psi_\xi}\frac{\partial \boldsymbol{\xi}}{\partial x_1} - \boldsymbol{I}_2\tilde{\boldsymbol{\mathcal{A}}}^{\langle k\rangle}_{\Psi_\xi}\frac{\partial \boldsymbol{\xi}}{\partial x_2}\end{aligned} \tag{24c}$$

$$\boldsymbol{H}^{\langle k\rangle}_n = -\sum_{i,\alpha}\frac{\partial \tilde{\boldsymbol{\mathcal{A}}}^{\langle ki\rangle}_{\Psi_\varepsilon\alpha}}{\partial x_3}\boldsymbol{\mathcal{D}}_p \boldsymbol{u}^{\langle i\rangle}_\alpha - \sum_{i,\lambda}\frac{\partial \tilde{\boldsymbol{\mathcal{A}}}^{\langle ki\rangle}_{\Psi_\tau\lambda}}{\partial x_3}\boldsymbol{\tau}^{\langle i\rangle}_\lambda - \frac{\partial \tilde{\boldsymbol{\mathcal{A}}}^{\langle k\rangle}_{\Psi_\xi}}{\partial x_3}\boldsymbol{\xi} \tag{24d}$$

where $\boldsymbol{I}_1^T = \begin{bmatrix}1 & 0\end{bmatrix}$ and $\boldsymbol{I}_2^T = \begin{bmatrix}0 & 1\end{bmatrix}$.

3.3. Layer governing equations

Considering that the Gauss' laws for electrostatics and magnetostatics are fulfilled in their strong form by the expressions of Φ and Ψ determined in the preceding section via Eqs.(14), the first variation of the functional Π reduces to its mechanical part only. For the k-th layer, the stationarity condition is then

written as

$$\begin{aligned}\delta\Pi^{\langle k\rangle} = &\int_{\Omega^{\langle k\rangle}}\int_{h_{k-1}}^{h_k}\left[\delta\boldsymbol{\varepsilon}^{\langle k\rangle\,T}\boldsymbol{\sigma}^{\langle k\rangle}+\delta\boldsymbol{\gamma}^{\langle k\rangle\,T}\boldsymbol{\tau}^{\langle k\rangle}\right]dx_3\,d\Omega+\\ &\int_{\Omega^{\langle k\rangle}}\int_{h_{k-1}}^{h_k}\delta\boldsymbol{\tau}^{\langle k\rangle\,T}\left(\boldsymbol{\gamma}^{\langle k\rangle}-\hat{\boldsymbol{\gamma}}^{\langle k\rangle}\right)dx_3\,d\Omega+\\ &\int_{\Omega^{\langle k\rangle}}\int_{h_{k-1}}^{h_k}\rho^{\langle k\rangle}\delta\boldsymbol{u}^{\langle k\rangle\,T}\ddot{\boldsymbol{u}}^{\langle k\rangle}\,dx_3\,d\Omega-\\ &\int_{\Omega^{\langle k\rangle}}\int_{h_{k-1}}^{h_k}\delta\boldsymbol{u}^{\langle k\rangle\,T}\bar{\boldsymbol{f}}^{\langle k\rangle}\,dx_3\,d\Omega-\int_{\partial\Omega^{\langle k\rangle}}\int_{h_{k-1}}^{h_k}\delta\boldsymbol{u}^{\langle k\rangle\,T}\bar{\boldsymbol{t}}_n^{\langle k\rangle}\,dx_3\,d\partial\Omega-\\ &\int_{\Omega^{\langle k\rangle}}\left[\left(\delta\boldsymbol{u}^{\langle k\rangle\,T}\bar{\boldsymbol{t}}_{x_3}^{\langle k\rangle}\right)\Big|_{h_k}+\left(\delta\boldsymbol{u}^{\langle k\rangle\,T}\bar{\boldsymbol{t}}_{x_3}^{\langle k\rangle}\right)\Big|_{h_{k-1}}\right]d\Omega=0\end{aligned}\tag{25}$$

where the integration domain $\Omega^{\langle k\rangle}\equiv\Omega$ is the reference plane of the lamina, $\bar{\boldsymbol{t}}_n^{\langle k\rangle}$ are the tractions applied on the layer lateral surfaces and $\bar{\boldsymbol{t}}_{x_3}^{\langle k\rangle}$ denotes tractions acting on planes parallel to Ω. The notation $f\,|_z$ is used to indicate that the function f is evaluated at $x_3=z$. It is worth noting that $\bar{\boldsymbol{t}}_{x_3}^{\langle 1\rangle}|_{h_0=-H/2}$ and $\bar{\boldsymbol{t}}_{x_3}^{\langle N\rangle}|_{h_N=H/2}$ coincide with the external tractions applied over the plate bottom and top surfaces, respectively.

The discrete form of Eq.(25) is obtained according to the following steps. First, the constitutive relationships from Eqs.(7) are substituted into Eq.(25). In turn, the gradient equations, namely Eqs.(13) and (24), are introduced and eventually the primary variables are expressed through their approximations, namely Eqs.(12).

Integrating by parts the resulting expression, one obtains the RMVT stationar-

ity statement for the k-th layer that reads

$$
\begin{aligned}
&-\int_{\Omega^{\langle k\rangle}}\sum_{\alpha}\delta\boldsymbol{u}_{\alpha}^{\langle k\rangle^T}\left[\sum_{i,\beta}{}^{u}_{\delta u}\boldsymbol{\mathcal{K}}_{\alpha\beta}^{\langle ki\rangle}\boldsymbol{u}_{\beta}^{\langle i\rangle}+\sum_{i,\mu}{}^{\tau}_{\delta u}\boldsymbol{\mathcal{K}}_{\alpha\mu}^{\langle ki\rangle}\boldsymbol{\tau}_{\mu}^{\langle i\rangle}\right]d\Omega-\int_{\Omega^{\langle k\rangle}}\sum_{\alpha}\delta\boldsymbol{u}_{\alpha}^{\langle k\rangle^T}{}^{\xi}_{\delta u}\boldsymbol{\mathcal{W}}_{\alpha}^{\langle k\rangle}\boldsymbol{\xi}\,d\Omega+\\
&\int_{\Omega^{\langle k\rangle}}\sum_{\lambda}\delta\boldsymbol{\tau}_{\lambda}^{\langle k\rangle^T}\left[\sum_{i,\beta}{}^{u}_{\delta\tau}\boldsymbol{\mathcal{K}}_{\lambda\mu}^{\langle ki\rangle}\boldsymbol{u}_{\mu}^{\langle i\rangle}+\sum_{i,\mu}{}^{\tau}_{\delta\tau}\boldsymbol{\mathcal{K}}_{\lambda\mu}^{\langle ki\rangle}\boldsymbol{\tau}_{\mu}^{\langle i\rangle}\right]d\Omega+\int_{\Omega^{\langle k\rangle}}\sum_{\lambda}\delta\boldsymbol{\tau}_{\lambda}^{\langle k\rangle^T}{}^{\xi}_{\delta\tau}\boldsymbol{\mathcal{W}}_{\lambda}^{\langle k\rangle}\boldsymbol{\xi}d\Omega+\\
&\int_{\partial\Omega^{\langle k\rangle}}\sum_{\alpha}\delta\boldsymbol{u}_{\alpha}^{\langle k\rangle^T}\left[\sum_{i,\beta}{}^{u}_{\delta u}\widetilde{\boldsymbol{\mathcal{K}}}_{\alpha\beta}^{\langle ki\rangle}\boldsymbol{u}_{\beta}^{\langle i\rangle}+\sum_{i,\mu}{}^{\tau}_{\delta u}\widetilde{\boldsymbol{\mathcal{K}}}_{\alpha\mu}^{\langle ki\rangle}\boldsymbol{\tau}_{\mu}^{\langle i\rangle}\right]d\partial\Omega+\int_{\partial\Omega^{\langle k\rangle}}\sum_{\alpha}\delta\boldsymbol{u}_{\alpha}^{\langle k\rangle^T}{}^{\xi}_{\delta u}\widetilde{\boldsymbol{\mathcal{W}}}_{\alpha}^{\langle k\rangle}\boldsymbol{\xi}\,d\partial\Omega+\\
&\int_{\Omega}\sum_{\alpha}\delta\boldsymbol{u}_{\alpha}^{\langle k\rangle^T}\sum_{\beta}{}^{u}_{\delta u}\boldsymbol{\mathcal{M}}_{\alpha\beta}^{\langle kk\rangle}\ddot{\boldsymbol{u}}_{\beta}^{\langle k\rangle}d\Omega-\int_{\Omega}\sum_{\alpha}\delta\boldsymbol{u}_{\alpha}^{\langle k\rangle^T}\left[\boldsymbol{\mathcal{F}}_{\alpha}^{\langle k\rangle}+\bar{\bar{\boldsymbol{\mathcal{P}}}}_{\alpha}^{\langle k\rangle}+\bar{\boldsymbol{\mathcal{P}}}_{\alpha}^{\langle k\rangle}\right]d\Omega-\\
&\int_{\partial\Omega}\sum_{\alpha}\delta\boldsymbol{u}_{\alpha}^{\langle k\rangle^T}\boldsymbol{\mathcal{T}}_{\alpha}^{\langle k\rangle}d\Omega=0
\end{aligned}
\tag{26}
$$

where the so-called *fundamental nuclei* [32] are defined as

$$
{}^{u}_{\delta u}\boldsymbol{\mathcal{K}}_{\alpha\beta}^{\langle ki\rangle}={}^{\varepsilon}_{\delta u}\boldsymbol{\mathcal{Q}}_{\alpha\beta}^{\langle ki\rangle}\boldsymbol{\mathcal{D}}_{p}^{T}\boldsymbol{\mathcal{D}}_{p} \tag{27a}
$$

$$
{}^{\tau}_{\delta u}\boldsymbol{\mathcal{K}}_{\alpha\mu}^{\langle ki\rangle}={}^{\tau}_{\delta u}\boldsymbol{\mathcal{Q}}_{\alpha\mu}^{\langle ki\rangle}+{}^{\tau}_{\delta\varepsilon}\boldsymbol{\mathcal{Q}}_{\alpha\mu}^{\langle ki\rangle}\boldsymbol{\mathcal{D}}_{p}^{T}\boldsymbol{\mathcal{D}}_{p}+{}^{\tau}_{\delta\gamma}\boldsymbol{\mathcal{Q}}_{\alpha\mu}^{\langle ki\rangle}\boldsymbol{\mathcal{D}}_{n}^{T}\boldsymbol{\mathcal{D}}_{n} \tag{27b}
$$

$$
\begin{aligned}
{}^{u}_{\delta\tau}\boldsymbol{\mathcal{K}}_{\lambda\beta}^{\langle ki\rangle}=&{}^{\varepsilon}_{\delta\tau}\boldsymbol{\mathcal{Q}}_{\lambda\beta}^{\langle ki\rangle}\boldsymbol{\mathcal{D}}_{p}+{}^{\gamma}_{\delta\tau}\boldsymbol{\mathcal{Q}}_{\lambda\beta}^{\langle ki\rangle}\boldsymbol{\mathcal{D}}_{n}+{}^{u}_{\delta\tau}\boldsymbol{\mathcal{Q}}_{\lambda\beta}^{\langle ki\rangle}+\\
&{}^{\frac{\partial\varepsilon}{\partial x_1}}_{\delta\tau}\boldsymbol{\mathcal{Q}}_{\lambda\beta}^{\langle ki\rangle}\frac{\partial}{\partial x_1}\boldsymbol{\mathcal{D}}_{p}+{}^{\frac{\partial\varepsilon}{\partial x_2}}_{\delta\tau}\boldsymbol{\mathcal{Q}}_{\lambda\beta}^{\langle ki\rangle}\frac{\partial}{\partial x_2}\boldsymbol{\mathcal{D}}_{p}
\end{aligned}
\tag{27c}
$$

$$
{}^{\tau}_{\delta\tau}\boldsymbol{\mathcal{K}}_{\lambda\mu}^{\langle ki\rangle}={}^{\tau}_{\delta\tau}\boldsymbol{\mathcal{Q}}_{\lambda\mu}^{\langle ki\rangle}+{}^{\frac{\partial\tau}{\partial x_1}}_{\delta\tau}\boldsymbol{\mathcal{Q}}_{\lambda\mu}^{\langle ki\rangle}\frac{\partial}{\partial x_1}+{}^{\frac{\partial\tau}{\partial x_1}}_{\delta\tau}\boldsymbol{\mathcal{Q}}_{\lambda\mu}^{\langle ki\rangle}\frac{\partial}{\partial x_2} \tag{27d}
$$

$$
{}^{u}_{\delta u}\boldsymbol{\mathcal{M}}_{\alpha\beta}^{\langle kk\rangle}=\boldsymbol{\mathcal{J}}_{\alpha\beta}^{\langle k\rangle} \tag{27e}
$$

$$
{}^{u}_{\delta u}\widetilde{\boldsymbol{\mathcal{K}}}_{\alpha\beta}^{\langle ki\rangle}=\widetilde{\boldsymbol{\mathcal{D}}}_{p}^{T}{}^{\varepsilon}_{\delta\varepsilon}\boldsymbol{\mathcal{Q}}_{\alpha\beta}^{\langle ki\rangle}\boldsymbol{\mathcal{D}}_{p} \tag{27f}
$$

$$
{}^{\tau}_{\delta u}\widetilde{\boldsymbol{\mathcal{K}}}_{\alpha\mu}^{\langle ki\rangle}=\widetilde{\boldsymbol{\mathcal{D}}}_{p}^{T}{}^{\tau}_{\delta\varepsilon}\boldsymbol{\mathcal{Q}}_{\alpha\mu}^{\langle ki\rangle}+\widetilde{\boldsymbol{\mathcal{D}}}_{n}^{T}{}^{\tau}_{\delta\gamma}\boldsymbol{\mathcal{Q}}_{\alpha\mu}^{\langle ki\rangle} \tag{27g}
$$

In Eq.(26), the electric and magnetic effective loading vectors are given by

$$
{}^{\xi}_{\delta u}\boldsymbol{\mathcal{W}}_{\alpha}^{\langle k\rangle}=\boldsymbol{\mathcal{D}}_{p}^{T}{}^{\xi}_{\delta\varepsilon}\boldsymbol{\mathcal{Q}}_{\alpha}^{\langle k\rangle} \tag{28a}
$$

$$
{}^{\xi}_{\delta u}\widetilde{\boldsymbol{\mathcal{W}}}_{\alpha}^{\langle k\rangle}=\widetilde{\boldsymbol{\mathcal{D}}}_{p}^{T}{}^{\xi}_{\delta\varepsilon}\boldsymbol{\mathcal{Q}}_{\alpha}^{\langle k\rangle} \tag{28b}
$$

$$\underset{\delta\tau}{\overset{\xi}{\boldsymbol{\mathcal{W}}}}{}_{\lambda}^{\langle k\rangle} = \underset{\delta\tau}{\overset{\xi}{\boldsymbol{Q}}}{}_{\lambda}^{\langle k\rangle} + \underset{\delta\tau}{\overset{\frac{\partial\xi}{\partial x_1}}{\boldsymbol{Q}}}{}_{\lambda}^{\langle k\rangle}\frac{\partial}{\partial x_1} + \underset{\delta\tau}{\overset{\frac{\partial\xi}{\partial x_2}}{\boldsymbol{Q}}}{}_{\lambda}^{\langle k\rangle}\frac{\partial}{\partial x_2} \tag{28c}$$

and the mechanical loading vectors read as

$$\bar{\boldsymbol{\mathcal{P}}}_{\alpha}^{\langle k\rangle} = \left| F_{\alpha}^{\langle k\rangle}\bar{\boldsymbol{t}}_{x_3}^{\langle k\rangle}\right|_{h_{k-1}} \tag{29a}$$

$$\bar{\bar{\boldsymbol{\mathcal{P}}}}_{\alpha}^{\langle k\rangle} = \left| F_{\alpha}^{\langle k\rangle}\bar{\boldsymbol{t}}_{x_3}^{\langle k\rangle}\right|_{h_{k}} \tag{29b}$$

$$\boldsymbol{\mathcal{F}}_{\alpha}^{\langle k\rangle} = \int_{h_{k-1}}^{h_k} F_{\alpha}^{\langle k\rangle}\bar{\boldsymbol{f}}^{\langle\kappa\rangle}dx_3 \tag{29c}$$

$$\boldsymbol{\mathcal{T}}_{\alpha}^{\langle k\rangle} = \int_{h_{k-1}}^{h_k} F_{\alpha}^{\langle k\rangle}\bar{\boldsymbol{t}}^{\langle k\rangle}dx_3 \tag{29d}$$

The expressions of the smart layer's effective characteristic matrices $\underset{r}{\overset{s}{\boldsymbol{Q}}}{}_{\omega\varsigma}^{\langle pq\rangle}$, effective inertia characteristics $\boldsymbol{J}_{\omega\varsigma}^{\langle k\rangle}$ and electric-magnetic effective loading characteristics $\underset{r}{\overset{s}{\boldsymbol{Q}}}{}_{\omega}^{\langle p\rangle}$ are given in Appendix B. In general, in the notation $\underset{g}{\overset{f}{\boldsymbol{B}}}{}_{\alpha\beta}^{\langle mn\rangle}$, f and g indicate specific fields, α and β indicate specific terms of the expansions of the above fields and m and n indicate specific layers within the laminate; in particular, the expansion term α of the field g within the layer m and the expansion term β of the field f within the layer n are being considered. Therefore, the fundamental nucleus $\underset{r}{\overset{s}{\boldsymbol{\mathcal{K}}}}{}_{\omega\varsigma}^{\langle pq\rangle}$ accounts for the contribution of the expansion term ω of the field r within the layer p to the work associated with the variation of the term ς of the field s within the layer q. On the other hand, the electric-magnetic loading kernel $\underset{r}{\overset{\xi}{\boldsymbol{\mathcal{W}}}}{}_{\omega}^{\langle p\rangle}$ accounts for the contribution of the electric-magnetic loading term $\boldsymbol{\xi}$ within the layer p to the work associated with the variation of the expansion term ω of the field r within the layer p itself.

Through standard calculus of variations on the stationarity statement given by Eq.(26), the layer governing equations holding in $\Omega^{\langle k\rangle}$ are eventually obtained

as

$$\begin{cases} \sum\limits_{i,\beta} {}^{u}_{\delta u}\boldsymbol{\mathcal{K}}^{\langle ki\rangle}_{\alpha\beta}\,\boldsymbol{u}^{\langle i\rangle}_{\beta} + \sum\limits_{i,\mu} {}^{\tau}_{\delta u}\boldsymbol{\mathcal{K}}^{\langle ki\rangle}_{\alpha\mu}\boldsymbol{\tau}^{\langle i\rangle}_{\mu} + \\ \qquad\qquad \sum\limits_{\beta} {}^{u}_{\delta u}\boldsymbol{\mathcal{M}}^{\langle k\rangle}_{\alpha\beta}\ddot{\boldsymbol{u}}^{\langle k\rangle}_{\beta} + {}^{\xi}_{\delta u}\boldsymbol{\mathcal{W}}^{\langle k\rangle}_{\alpha}\boldsymbol{\xi} - \boldsymbol{\mathcal{F}}^{\langle k\rangle}_{\alpha} - \bar{\bar{\boldsymbol{\mathcal{P}}}}^{\langle k\rangle}_{\alpha} - \bar{\boldsymbol{\mathcal{P}}}^{\langle k\rangle}_{\alpha} = \boldsymbol{0} \\ \sum\limits_{i,\beta} {}^{u}_{\delta\tau}\boldsymbol{\mathcal{K}}^{\langle ki\rangle}_{\lambda\beta}\,\boldsymbol{u}^{\langle i\rangle}_{\beta} + \sum\limits_{i,\mu} {}^{\tau}_{\delta\tau}\boldsymbol{\mathcal{K}}^{\langle ki\rangle}_{\lambda\mu}\boldsymbol{\tau}^{\langle i\rangle}_{\mu} + {}^{\xi}_{\delta\tau}\boldsymbol{\mathcal{W}}^{\langle k\rangle}_{\alpha}\boldsymbol{\xi} = \boldsymbol{0} \end{cases} \tag{30}$$

with $\alpha = 1, 2, ..., M_u$ and $\lambda = 1, 2, ..., M_\tau$; the associated natural boundary conditions, holding on $\partial\Omega^{\langle k\rangle}$, are given by

$$\sum_{i,\beta} {}^{u}_{\delta u}\widehat{\boldsymbol{\mathcal{K}}}^{\langle ki\rangle}_{\alpha\beta}\,\boldsymbol{u}^{\langle i\rangle}_{\beta} + \sum_{i,\mu} {}^{\tau}_{\delta u}\widehat{\boldsymbol{\mathcal{K}}}^{\langle ki\rangle}_{\alpha\mu}\boldsymbol{\tau}^{\langle i\rangle}_{\mu} + {}^{\xi}_{\delta u}\widehat{\boldsymbol{\mathcal{W}}}^{\langle k\rangle}_{\alpha}\boldsymbol{\xi} - \boldsymbol{T}^{\langle k\rangle}_{\alpha} = \boldsymbol{0}. \tag{31}$$

4. Multilayered plate

The governing equations for multilayered plates are obtained by enforcing the stationarity condition of the functional Π for all the laminate layers

$$\sum_{k=1}^{n} \delta\Pi^{\langle k\rangle} = 0 \tag{32}$$

with the additional requirements on the interface displacements continuity and tractions equilibrium

$$\begin{cases} \boldsymbol{u}^{\langle k\rangle}\Big|_{h_k} - \boldsymbol{u}^{\langle k+1\rangle}\Big|_{h_k} = \boldsymbol{0} \qquad k = 1, 2, \ldots, (N-1) \\ \bar{\boldsymbol{t}}^{\langle k\rangle}_{x_3}\Big|_{h_k} + \bar{\boldsymbol{t}}^{\langle k+1\rangle}_{x_3}\Big|_{h_k} = \boldsymbol{0} \qquad \kappa = 1, 2, \ldots, (N-1) \end{cases} \tag{33}$$

Enforcing the stationarity and interface conditions in Eqs.(32-33) leads to the plate resolving system

$$\begin{aligned} \boldsymbol{K}_{uu}\boldsymbol{U} + \boldsymbol{K}_{u\tau}\boldsymbol{T} &= \boldsymbol{F}_u - \boldsymbol{M}_{uu}\ddot{\boldsymbol{U}} \\ \boldsymbol{K}_{\tau u}\boldsymbol{U} + \boldsymbol{K}_{\tau\tau}\boldsymbol{T} &= \boldsymbol{F}_\tau \end{aligned} \tag{34}$$

where $\boldsymbol{U}$ and $\boldsymbol{T}$ are vectors collecting the the unknown coefficients of the displacement and transverse stress expansions $\boldsymbol{u}_\alpha^{\langle\kappa\rangle}$ and $\boldsymbol{\tau}_\lambda^{\langle\kappa\rangle}$ and the operator matrices $\boldsymbol{K}_{rs}$ $(r,s=u,\tau)$, $\boldsymbol{M}_{uu}$ and the loading vectors $\boldsymbol{F}_r$ $(r=u,\tau)$ are obtained via assembly procedures of the fundamental nuclei, which are described in the next sections.

4.1. Layer-wise theories

Assuming the primary variable expansion coefficients $\boldsymbol{u}_\alpha^{\langle\kappa\rangle}$ and $\boldsymbol{\tau}_\lambda^{\langle\kappa\rangle}$ as distinct for each individual layer leads to layer-wise plate models. In this case, a suitable choice of the thickness functions F_α is a linear combination of Legendre polynomials $\mathscr{L}_\alpha(\zeta_k)$ specified as

$$F_0^{\langle\kappa\rangle} = \frac{\mathscr{L}_0(\zeta_k) - \mathscr{L}_1(\zeta_k)}{2} \tag{35}$$

$$F_\alpha^{\langle\kappa\rangle} = \mathscr{L}_{\alpha+1}(\zeta_k) - \mathscr{L}_{\alpha-1}(\zeta_k) \qquad \alpha = 1,...(M-1) \tag{36}$$

$$F_M^{\langle\kappa\rangle} = \frac{\mathscr{L}_0(\zeta_k) + \mathscr{L}_1(\zeta_k)}{2} \tag{37}$$

where $\zeta_k = (2x_3 - h_\kappa - h_{\kappa-1}) / (h_\kappa - h_{\kappa-1})$ (see Fig. 1). The same choice is introduced for the transverse stress thickness functions $\tilde{F}_\lambda$. Due to the properties of the Legendre polynomials, the displacements continuity and tractions equilibrium at the layer interfaces reduce to the following relationships

$$\begin{aligned} \boldsymbol{u}_{M_u}^{\langle k\rangle} &= \boldsymbol{u}_0^{\langle k+1\rangle} \\ \boldsymbol{\tau}_{M_\tau}^{\langle k\rangle} &= \boldsymbol{\tau}_0^{\langle k+1\rangle} \end{aligned} \qquad k = 1,\dots,(N-1). \tag{38}$$

Taking Eqs.(38) into account, the unknown primary variables can be collected into the global column vectors $\boldsymbol{U}$, whose rows with indexes ranging from $3[(k-1)M_u+\alpha+1]-2$ to $3[(k-1)M_u+\alpha+1]$ contain the coefficients $\boldsymbol{u}_\alpha^{\langle k\rangle}$, and $\boldsymbol{T}$, whose rows with indexes ranging from $3[(k-1)M_\tau+\alpha+1]-2$ to $3[(k-1)M_\tau+\alpha+1]$ contain the coefficients $\boldsymbol{\tau}_\alpha^{\langle k\rangle}$.

According with this global indexing of the unknown coefficients, the resolving system matrices $\boldsymbol{K}_{rs}$ are built by summing the fundamental nuclei ${}_{\delta r}^{s}\boldsymbol{\mathcal{K}}_{\omega\varsigma}^{\langle ki\rangle}$ at the

rows with indexes ranging from $3[(k-1)M_r+\omega+1]-2$ to $3[(k-1)M_r+\omega+1]$ and the columns with indexes ranging from $3[(i-1)M_s+\varsigma+1]-2$ to $3[(i-1)M_s+\varsigma+1]$. Similarly, the matrix $\boldsymbol{M}_{uu}$ is built by summing the fundamental nuclei ${}^{u}_{\delta u}\mathfrak{M}^{\langle ki\rangle}_{\omega\varsigma}$ at the rows with indexes ranging from $3[(k-1)M_u+\omega+1]-2$ to $3[(k-1)M_u+\omega+1]$ and the columns with indexes ranging from $3[(i-1)M_u+\varsigma+1]-2$ to $3[(i-1)M_u+\varsigma+1]$. The right-hand-side vector $\boldsymbol{F}_u$ is built by: *a*) summing the nuclei ${}^{\xi}_{\delta u}\mathbf{W}^{\langle k\rangle}_{\omega}$ and the domain load terms $\boldsymbol{F}^{\langle k\rangle}_{\omega}$ at the rows from $3[(k-1)M_u+\omega+1]-2$ to $3[(k-1)M_u+\omega+1]$; *b*) summing at the rows from 1 to 3 the nucleus $\bar{\boldsymbol{\mathcal{P}}}^{\langle 1\rangle}_{0}$ accounting for the external mechanical load $\bar{\boldsymbol{t}}^{\langle 1\rangle}_{x_3}|_{-h/2}$ applied at the laminate bottom surface; *c*) summing at the rows from $3(NM_u+1)-2$ to $3(NM_u+1)$ the nucleus $\bar{\boldsymbol{\mathcal{P}}}^{\langle N\rangle}_{M_u}$ accounting for the external mechanical load $\bar{\boldsymbol{t}}^{\langle N\rangle}_{x_3}|_{h/2}$ applied at the laminate top surface Finally, the right-hand-side vector $\boldsymbol{F}_\tau$ is built by summing the nuclei ${}^{\xi}_{\delta\tau}\mathbf{W}^{\langle k\rangle}_{\omega}$ at the rows from from $3[(k-1)M_r+\omega+1]-2$ to $3[(k-1)M_r+\omega+1]$. It is worth noting that $\bar{\boldsymbol{t}}^{\langle 1\rangle}_{x_3}|_{-h/2}=\boldsymbol{\tau}^{\langle 1\rangle}_{0}$ and $\bar{\boldsymbol{t}}^{\langle N\rangle}_{x_3}|_{h/2}=\boldsymbol{\tau}^{\langle N\rangle}_{M_\tau}$; this represents a constraint for the transverse stress expansion coefficients, which can be forced in the resolving system through penalty techniques.

4.2. Equivalent-single-layer theories

For the equivalent-single-layer plate models, the primary variable expansion coefficients $\boldsymbol{u}^{\langle\kappa\rangle}_{\alpha}=\boldsymbol{u}_\alpha$ are assumed common to the all of the layers whereas the expansion coefficients $\boldsymbol{\tau}^{\langle\kappa\rangle}_{\lambda}$ are again assumed as distinct for each individual layer. In this case, a suitable choice of the thickness functions $F^{\langle k\rangle}_{\alpha}$ is provided by the adoption of Taylor polynomials

$$F^{\langle\kappa\rangle}_{\alpha}=x_3^{\alpha}, \qquad \alpha=0,...,M_u. \tag{39}$$

The thickness functions $\tilde{F}^{\langle k\rangle}_{\lambda}$ are defined by Eq.(35). Due to the thickness functions selections, the displacements continuity and tractions equilibrium at

the layer interfaces reduce to the following relationships

$$\begin{aligned} \boldsymbol{u}_{\alpha}^{\langle k \rangle} &= \boldsymbol{u}_{\alpha}^{\langle k+1 \rangle} \\ \boldsymbol{\tau}_{M_\tau}^{\langle k \rangle} &= \boldsymbol{\tau}_{0}^{\langle k+1 \rangle} \end{aligned} \qquad \begin{aligned} &with \\ \end{aligned} \qquad \begin{aligned} &\alpha = 0, \ldots, M_u \\ &k = 1, \ldots, (N-1) \end{aligned} \tag{40}$$

The displacement expansion coefficients are then collected within the global column vector $\boldsymbol{U}$, whose rows with indexes ranging from $3[\alpha+1]-2$ to $3[\alpha+1]$ contain the coefficients $\boldsymbol{u}_\alpha$ and the transverse stress expansion coefficients are collected within the vector $\boldsymbol{T}$, whose rows with indexes ranging from $3[(k-1)M_\tau+\alpha+1]-2$ to $3[(k-1)M_\tau+\alpha+1]$ contain $\boldsymbol{\tau}_{\alpha}^{\langle k \rangle}$.

According with this global indexing of the unknown coefficients the resolving system matrices are built as follows. The matrices $\boldsymbol{K}_{uu}$ and $\boldsymbol{M}_{uu}$ are built by summing the fundamental nuclei ${}^{u}_{\delta u}\boldsymbol{\mathcal{K}}^{\langle ki \rangle}_{\omega\varsigma}$ and ${}^{u}_{\delta u}\boldsymbol{\mathcal{M}}^{\langle kk \rangle}_{\omega\varsigma}$, respectively, at the rows with indexes ranging from $3[\omega+1]-2$ to $3[\omega+1]$ and the columns with indexes ranging from $3[\varsigma+1]-2$ to $3[\varsigma+1]$.

The matrix $\boldsymbol{K}_{u\tau}$ is built by summing the fundamental nuclei ${}^{\tau}_{\delta u}\boldsymbol{\mathcal{K}}^{\langle ki \rangle}_{\omega\varsigma}$ at the rows with indexes ranging from $3[(\omega+1]-2$ to $3[\omega+1]$ and the columns with indexes ranging from $3[(i-1)M_\tau+\varsigma+1]-2$ to $3[(i-1)M_\tau+\varsigma+1]$.

The matrix $\boldsymbol{K}_{\tau u}$ is built by summing the fundamental nuclei ${}^{u}_{\delta \tau}\boldsymbol{\mathcal{K}}^{\langle ki \rangle}_{\omega\varsigma}$ at the rows with indexes ranging from $3[(k-1)M_\tau+\omega+1]-2$ to $3[(k-1)M_\tau+\omega+1]$ and the columns with indexes ranging from $3[\varsigma+1]-2$ to $3[\varsigma+1]$.

The matrix $\boldsymbol{K}_{\tau\tau}$ is built by summing the fundamental nuclei ${}^{\tau}_{\delta \tau}\boldsymbol{\mathcal{K}}^{\langle ki \rangle}_{\omega\varsigma}$ at the rows with indexes ranging from $3[(k-1)M_\tau+\omega+1]-2$ to $3[(k-1)M_\tau+\omega+1]$ and the columns with indexes ranging from $3[(i-1)M_\tau+\varsigma+1]-2$ to $3[(i-1)M_\tau+\varsigma+1]$.

The right-hand-side vector $\boldsymbol{F}_u$ is built by summing the nuclei ${}^{\xi}_{\delta u}\boldsymbol{\mathcal{W}}^{\langle k \rangle}_{\omega}$, the domain load terms $\boldsymbol{F}^{\langle k \rangle}_{\omega}$ and the external surface load characteristics $\bar{\boldsymbol{P}}^{\langle 1 \rangle}_{\omega}$ and $\bar{\bar{\boldsymbol{P}}}^{\langle N \rangle}_{\omega}$ at the rows with indexes ranging from $3[\omega+1]-2$ to $3[\omega+1]$.

Finally, the right-hand-side vector $\boldsymbol{F}_\tau$ is built by summing the nuclei ${}^{\xi}_{\delta \tau}\boldsymbol{\mathcal{W}}^{\langle k \rangle}_{\omega}$ at the rows with indexes ranging from $3[(k-1)M_r+\omega+1]-2$ to $3[(k-1)M_r+\omega+1]$.

Also in this case, the transverse stress expansion coefficients constraints, expressed by $\bar{\boldsymbol{t}}^{\langle 1 \rangle}_{x_3}|_{-h/2} = \boldsymbol{\tau}^{\langle 1 \rangle}_{0}$ and $\bar{\boldsymbol{t}}^{\langle N \rangle}_{x_3}|_{h/2} = \boldsymbol{\tau}^{\langle N \rangle}_{M_\tau}$, have to be be enforced.

5. Solution and results

Let us consider a simply-supported rectangular plate with MEE layers with principal material axes aligned with the plate reference system. In this case, a closed form solution can be found assuming the following expressions for the primary variable expansion terms

$$\boldsymbol{u}_{\alpha}^{\langle k\rangle} = \left\{ \begin{array}{l} \sum_{m}\sum_{n} {u_1}_{\alpha\, mn}^{\langle k\rangle} \cos\dfrac{m\pi}{L_x}x_1 \ \sin\dfrac{n\pi}{L_y}x_2 \\ \sum_{m}\sum_{n} {u_2}_{\alpha\, mn}^{\langle k\rangle} \sin\dfrac{m\pi}{L_x}x_1 \ \cos\dfrac{n\pi}{L_y}x_2 \\ \sum_{m}\sum_{n} {u_3}_{\alpha\, mn}^{\langle k\rangle} \sin\dfrac{m\pi}{L_x}x_1 \ \sin\dfrac{n\pi}{L_y}x_2 \end{array} \right\} \exp\left(\sqrt{-1}\varpi t\right), \tag{41a}$$

$$\boldsymbol{\tau}_{\lambda}^{\langle k\rangle} = \left\{ \begin{array}{l} \sum_{m}\sum_{n} {\sigma_{31}}_{\lambda\, mn}^{\langle k\rangle} \cos\dfrac{m\pi}{L_x}x_1 \ \sin\dfrac{n\pi}{L_y}x_2 \\ \sum_{m}\sum_{n} {\sigma_{32}}_{\lambda\, mn}^{\langle k\rangle} \sin\dfrac{m\pi}{L_x}x_1 \ \cos\dfrac{n\pi}{L_y}x_2 \\ \sum_{m}\sum_{n} {\sigma_{33}}_{\lambda\, mn}^{\langle k\rangle} \sin\dfrac{m\pi}{L_x}x_1 \ \sin\dfrac{n\pi}{L_y}x_2 \end{array} \right\} \exp\left(\sqrt{-1}\varpi t\right). \tag{41b}$$

Substituting Eqs.(41) into the plate governing equations and applying the Bubnov-Galerkin method, an algebraic resolving system is obtained for the unknown coefficients ${u_j}_{\alpha\, mn}^{\langle k\rangle}$ and ${\sigma_{3j}}_{\lambda\, mn}^{\langle k\rangle}$ associated with each of the harmonic terms of the primary variables approximation series. In the present work, representative results obtained using the mentioned closed-form solution are presented and discussed. Different LW and ESL theories have been implemented considering variable kinematics with through-the-thickness power expansion orders up to the fourth.

Results are presented for smart MEE multilayered plates with plies of piezo-

electric barium titanate $BaTiO_3$ and piezomagnetic cobalt ferrite $CoFe_2O_4$, shortly denoted as B and F respectively, whose material properties can be found in Ref.[25]. Attention is devoted to thick plates, as these allow to highlight the possible lack of accuracy and the effectiveness of $2D$ plate theories. Thus, simply-supported square plates with side length $L_x = 1m$, total thickness $H = 0.3m$ and equal thickness layers $B/F/B$ and $F/B/F$ stacking sequences have been investigated as representative problem. However it is worth mentioning that the scheme has been used to analyse different lay-ups, obtaining similar results.

5.1. Static analysis under mechanical load

The plates undergo a bi-sinusoidal pressure $p_3 = \bar{p}_3 \sin(\pi x_1/L_x) \sin(\pi x_2/L_x)$ applied over the top surface with peak $\bar{p}_3 = 1N/m^2$. The electric and magnetic potentials are set to zero on both the top and bottom plate surfaces, which correspond to the closed circuit condition. For this problem the exact $3D$ solution can be evaluated by the approach given in Ref.[6]. First, a set of numerical experiments have been performed by selecting transverse stress expansions of order greater than, equal to and lower than that adopted for the displacements expansions. Fig.2 and Fig.3 show representative results for these analyses highlighting how the choice of the same expansion order for both displacements and transverse stresses provides reliable results for all the investigated theories. Indeed, it is observed that, for LW models, selecting for the transverse stresses expansions an order lower than that selected for the displacements provides good results for higher order theories only. On the other hand, for ESL models, selecting for the transverse stresses expansions an order greater than that selected for the displacements provides good results for higher order theories only.

To appraise the approach accuracy, Fig.4 and Fig.5 show the through-the-thickness distribution of representative mechanical and electric and magnetic quantities at the point of coordinates $x_1 = x_2 = 0.25L_x$ for different plate models and their comparison with the $3D$ exact solution. These results have been

obtained using the same expansion order for both displacements and transverse stresses. As expected, better results are obtained employing higher order layer-wise models, which provide accurate distributions of mechanical quantities and electric potential, whereas a slight loss of accuracy with respect to the analytic solution is shown for the magnetic potentials. Higher order ESL models can give satisfactory results and also in this case the magnetic potential results slightly overestimated with respect to the analytic solution.

5.2. Static analysis under electromagnetic load

A plate with $H/L_x = 0.1$ and the same lay-up as that considered in the previous example, subjected to a bi-sinusoidal electric voltage with peak $\Delta\Phi = 100V$, has been analysed; the voltage is symmetrically applied between the upper and bottom surfaces and zero magnetic potential is assumed over both the top and bottom plate surfaces. In this case the plate can be considered as an actuator under the action of the external electric excitation. Results for representative quantities of the plate response are shown in Fig.6 and Fig.7 for layer-wise and equivalent-single-layer theories, respectively. The analytic $3D$ solution, computed using the approach given in Ref.[6], is also shown. It is observed that the obtained results are generally in good agreement with those of the $3D$ solution with a slight overestimation of the magnetic quantities. As expected, also in this case, layer-wise theories generally deliver more reliable results with respect to those produced by equivalent-single-layer models and they are adequately accurate if higher order expansions are employed.

5.3. Free vibrations

Tables 1 and 2 list the first five natural frequency ϖ of the $B/F/B$ and $F/B/F$ simply-supported square plates related to spatial modes with $m = n = 1$ in Eq. (41). The plate circular frequencies are normalised as $\bar{\omega} = \varpi L_x \sqrt{\rho_{max}/C_{max}}$, where C_{max} and ρ_{max} are the maximum values of the elastic coefficient and density among the materials of the plate layers. Results are presented for both LW and ESL models, which are labeled by the acronyms

LWn and $ESLn$ being n the order of the employed thickness expansions, selected with the same order for both displacements and transverse stresses. Two different aspect ratios, namely $H/L_x = 0.1$ and $H/L_x = 0.3$, are investigated and closed circuit conditions, i.e. zero electric and magnetic potentials on both top and bottom plate surfaces, are enforced. Results are compared with those produced using the $3D$ approach given in Ref. [7]. The agreement between the two different solutions confirms the accuracy of the proposed approach. Both LW and ESL models give reliable natural frequencies and little or no difference is found between the predictions of the two techniques, which can be motivated by the fact that natural frequencies characterise the global behaviour of the plate that is not affected by slight differences in the local fields.

6. Conclusions

In the present work, advanced multilayered models for smart plates have been developed in the framework of an axiomatic unified formulation where the order of the through-the-thickness expansion is assumed as a model parameter at layer level. The proposed models are based on the condensation of the electric and magnetic states into the plate mechanics, performed via the strong form of the electrostatics and magnetostatics governing equations. Consequently, the plate governing equations are inferred by using the generalised Reissner Mixed Variational Theorem. The resulting layer model corresponds to an effective plate, with mechanical behaviour only, described in terms of suitable stiffness, inertia and loading characteristics that take the magneto-electro-elastic coupling into account. The layers equations are then coupled through the interface conditions that provide displacement and transverse stress continuity, which can be explicitly enforced thanks to the use of RMVT. The method naturally translates into through-the-thickness algorithmic assembly procedures that allow to build models based on both equivalent single layer and layer-wise kinematics. The approach has been validated against solutions available in the literature for static problems and free vibrations. The obtained results confirm good accuracy

and the potential of the approach for the construction of general smart laminate models.

7. References

[1] I. Chopra, Review of state of art of smart structures and integrated systems, AIAA Journal 40 (11) (2002) 2145–2187.

[2] C.-W. Nan, M. Bichurin, S. Dong, D. Viehland, G. Srinivasan, Multiferroic magnetoelectric composites: Historical perspective, status, and future directions, Journal of Applied Physics 103 (3).

[3] S. V. Gopinathan, V. V. Varadan, V. K. Varadan, A review and critique of theories for piezoelectric laminates, Smart Materials and Structures 9 (1) (2000) 24.

[4] J. Zhai, Z. Xing, S. Dong, J. Li, D. Viehland, Magnetoelectric laminate composites: An overview, Journal of the American Ceramic Society 91 (2) (2008) 351–358.

[5] S. Kapuria, P. Kumari, N. J.K., Efficient modeling of smart piezoelectric composite laminates: a review, Acta Mechanica 214 (2010) 31–48.

[6] E. Pan, Exact solution for simply supported and multilayered magneto-electro-elastic plates, Journal of Applied Mechanics, Transactions ASME 68 (4) (2001) 608–618.

[7] E. Pan, P. R. Heyliger, Free vibrations of simply supported and multilayered magneto-electro-elastic plates, Journal of Sound and Vibration 252 (3) (2002) 429 – 442.

[8] J. Wang, L. Chen, S. Fang, State vector approach to analysis of multilayered magneto-electro-elastic plates, International Journal of Solids and Structures 40 (7) (2003) 1669–1680.

[9] R. Bhangale, N. Ganesan, Static analysis of simply supported functionally graded and layered magneto-electro-elastic plates, International Journal of Solids and Structures 43 (10) (2006) 3230–3253.

[10] A. Milazzo, I. Benedetti, C. Orlando, Boundary element method for magneto electro elastic laminates, CMES - Computer Modeling in Engineering and Sciences 15 (1) (2006) 17–30.

[11] C.-P. Wu, Y.-C. Lu, A modified pagano method for the 3d dynamic responses of functionally graded magneto-electro-elastic plates, Composite Structures 90 (3) (2009) 363–372.

[12] I. Benedetti, A. Milazzo, M. Aliabadi, Structures with surface-bonded pzt piezoelectric patches: a bem investigation into the strain-transfer mechanism for shm applications, SDHM: Structural Durability & Health Monitoring 5 (3) (2009) 251–274.

[13] I. Benedetti, M. Aliabadi, A. Milazzo, A fast {BEM} for the analysis of damaged structures with bonded piezoelectric sensors, Computer Methods in Applied Mechanics and Engineering 199 (912) (2010) 490 – 501.

[14] G. Daví, A. Milazzo, A regular variational boundary model for free vibrations of magneto-electro-elastic structures, Engineering Analysis with Boundary Elements 35 (3) (2011) 303–312.

[15] M.-F. Liu, An exact deformation analysis for the magneto-electro-elastic fiber-reinforced thin plate, Applied Mathematical Modelling 35 (5) (2011) 2443–2461.

[16] Z. Yifeng, C. Lei, W. Yu, Z. Xiaopin, Z. Liangliang, Asymptotical construction of a reissner-like model for multilayer functionally graded magneto-electro-elastic plates, Composite Structures 96 (2013) 786–798.

[17] D. Sladek, V. Sladek, S. Krahulec, E. Pan, The mlpg analyses of large deflections of magnetoelectroelastic plates, Engineering Analysis with Boundary Elements 37 (2013) 673–682.

[18] J. Liu, P. Zhang, G. Lin, W. Wang, S. Lu, Solutions for the magneto-electro-elastic plate using the scaled boundary finite element method, Engineering Analysis with Boundary Elements 68 (2016) 103–114.

[19] F. Zou, I. Benedetti, M. H. Aliabadi, A boundary element model for structural health monitoring using piezoelectric transducers, Smart Materials and Structures 23 (1) 015022.

[20] R. Garcia Lage, C. M. Mota Soares, C. A. Mota Soares, J. N. Reddy, Layerwise partial mixed finite element analysis of magneto-electro-elastic plates, Computers & Structures 82 (17-19) (2004) 1293–1301.

[21] S. Phoenix, S. Satsangi, B. Singh, Layer-wise modelling of magneto-electro-elastic plates, Journal of Sound and Vibration 324 (3-5) (2009) 798–815.

[22] J. Simões Moita, C. Mota Soares, C. Mota Soares, Analyses of magneto-electro-elastic plates using a higher order finite element model, Composite Structures 91 (4) (2009) 421 – 426.

[23] M. Rao, R. Schmidt, K.-U. Schrder, Geometrically nonlinear static fe-simulation of multilayered magneto-electro-elastic composite structures, Composite Structures 127 (2015) 120–131.

[24] E. Carrera, S. Brischetto, P. Nali, Plates and Shells for Smart Structures: Classical and Advanced Theories for Modeling and Analysis, Wiley, 2011.

[25] A. Milazzo, An equivalent single-layer model for magnetoelectroelastic multilayered plate dynamics, Composite Structures 94 (6) (2012) 2078–2086.

[26] A. Alaimo, A. Milazzo, C. Orlando, A four-node mitc finite element for magneto-electro-elastic multilayered plates, Computers and Structures 129 (2013) 120–133.

[27] A. Alaimo, I. Benedetti, A. Milazzo, A finite element formulation for large deflection of multilayered magneto-electro-elastic plates, Composite Structures 107 (2014) 643–653.

[28] G. Altay, M. Dkmeci, On the fundamental equations of electromagnetoelastic media in variational form with an application to shell/laminae equations, International Journal of Solids and Structures 47 (3-4) (2010) 466–492.

[29] Z.-B. Kuang, Physical variational principle and thin plate theory in electromagneto-elastic analysis, International Journal of Solids and Structures 48 (2) (2011) 317–325.

[30] E. Reissner, On a certain mixed variational theorem and a proposed application, International Journal for Numerical Methods in Engineering 20 (7) (1984) 1366–1368.

[31] E. Reissner, On a mixed variational theorem and on shear deformable plate theory, International Journal for Numerical Methods in Engineering 23 (2) (1986) 193–198.

[32] E. Carrera, Theories and finite elements for multilayered plates and shells: A unified compact formulation with numerical assessment and benchmarking, Archives of Computational Methods in Engineering 10 (3) (2003) 215–296.

[33] E. Carrera, L. Demasi, Classical and advanced multilayered plate elements based upon pvd and rmvt. part 1: Derivation of finite element matrices, International Journal for Numerical Methods in Engineering 55 (2) (2002) 191–231.

[34] E. Carrera, M. Di Gifico, P. Nali, S. Brischetto, Refined multilayered plate elements for coupled magneto-electro-elastic analysis, Multidiscipline Modeling in Materials and Structures 5 (2) (2009) 119–138.

[35] E. Carrera, S. Brischetto, C. Fagiano, P. Nali, Mixed multilayered plate elements for coupled magneto-electro-elastic analysis, Multidiscipline Modeling in Materials and Structures 5 (3) (2009) 251 – 256.

[36] E. Carrera, P. Nali, Multilayered plate elements for the analysis of multifield problems, Finite Elements in Analysis and Design 46 (9) (2010) 732 – 742.

[37] A. Milazzo, Refined equivalent single layer formulations and finite elements for smart laminates free vibrations, Composites Part B: Engineering 61 (2014) 238–253.

[38] A. Milazzo, Layer-wise and equivalent single layer models for smart multilayered plates, Composites Part B: Engineering 67 (2014) 62–75.

[39] A. Milazzo, Variable kinematics models and finite elements for nonlinear analysis of multilayered smart plates, Composite Structures 122 (2015) 537–545.

[40] A. Milazzo, Unified formulation for a family of advanced finite elements for smart multilayered plates, Mechanics of Advanced Materials and Structures 23 (9) (2016) 971–980.

[41] M. D'Ottavio, B. Krplin, An extension of reissner mixed variational theorem to piezoelectric laminates, Mechanics of Advanced Materials and Structures 13 (2) (2006) 139–150.

[42] E. Carrera, S. Brischetto, P. Nali, Variational statements and computational models for multifield problems and multilayered structures, Mechanics of Advanced Materials and Structures 15 (3-4) (2008) 182–198.

Appendix A. Matrices of the mixed form MEE constitutive law

The matrices involved in the the mixed form of the MEE constitutive law, Eq.(7), are defined as

$$\boldsymbol{C}_{\sigma\varepsilon} = \boldsymbol{C}_{pp} - \boldsymbol{C}_{np}^{T}\boldsymbol{C}_{nn}^{-1}\boldsymbol{C}_{np} \tag{A.1}$$

$$\boldsymbol{C}_{\sigma\tau} = \boldsymbol{C}_{np}^{T}\boldsymbol{C}_{nn}^{-1} \tag{A.2}$$

$$\boldsymbol{C}_{\sigma E_n} = \boldsymbol{C}_{np}^{T}\boldsymbol{C}_{nn}^{-1}\boldsymbol{e}_{nn}^{T} - \boldsymbol{e}_{np}^{T} \tag{A.3}$$

$$\boldsymbol{C}_{\sigma H_n} = \boldsymbol{C}_{np}^{T}\boldsymbol{C}_{nn}^{-1}\boldsymbol{q}_{nn}^{T} - \boldsymbol{q}_{np}^{T} \tag{A.4}$$

$$\boldsymbol{C}_{\gamma\varepsilon} = -\boldsymbol{C}_{nn}^{-1}\boldsymbol{C}_{np} \tag{A.5}$$

$$\boldsymbol{C}_{\gamma\tau} = \boldsymbol{C}_{nn}^{-1} \tag{A.6}$$

$$\boldsymbol{C}_{\gamma E_p} = \boldsymbol{C}_{nn}^{-1}\boldsymbol{e}_{pn}^{T} \tag{A.7}$$

$$\boldsymbol{C}_{\gamma E_n} = \boldsymbol{C}_{nn}^{-1}\boldsymbol{e}_{nn}^{T} \tag{A.8}$$

$$\boldsymbol{C}_{\varepsilon_n H_p} = \boldsymbol{C}_{nn}^{-1}\boldsymbol{q}_{pn}^{T} \tag{A.9}$$

$$\boldsymbol{C}_{\gamma H_n} = \boldsymbol{C}_{nn}^{-1}\boldsymbol{q}_{nn}^{T} \tag{A.10}$$

$$\boldsymbol{C}_{D_p\tau} = \boldsymbol{e}_{pn}\boldsymbol{C}_{nn}^{-1} \tag{A.11}$$

$$\boldsymbol{C}_{D_p E_p} = \boldsymbol{e}_{pn}\boldsymbol{C}_{nn}^{-1}\boldsymbol{e}_{pn}^{T} + \boldsymbol{\epsilon}_{pp} \tag{A.12}$$

$$\boldsymbol{C}_{D_p H_p} = \boldsymbol{e}_{pn}\boldsymbol{C}_{nn}^{-1}\boldsymbol{q}_{pn}^{T} + \boldsymbol{\eta}_{pp} \tag{A.13}$$

$$\boldsymbol{C}_{D_n\varepsilon} = -\left(\boldsymbol{e}_{nn}\boldsymbol{C}_{nn}^{-1}\boldsymbol{C}_{np} - \boldsymbol{e}_{np}\right) \tag{A.14}$$

$$\boldsymbol{C}_{D_n\tau} = \boldsymbol{e}_{nn}\boldsymbol{C}_{nn}^{-1} \tag{A.15}$$

$$\boldsymbol{C}_{D_n E_n} = \boldsymbol{e}_{nn}\boldsymbol{C}_{nn}^{-1}\boldsymbol{e}_{nn}^{T} + \boldsymbol{\epsilon}_{nn} \tag{A.16}$$

$$\boldsymbol{C}_{D_n H_n} = \boldsymbol{e}_{nn}\boldsymbol{C}_{nn}^{-1}\boldsymbol{q}_{nn}^{T} + \boldsymbol{\eta}_{nn} \tag{A.17}$$

$$\boldsymbol{C}_{B_p\tau} = \boldsymbol{q}_{pn}\boldsymbol{C}_{nn}^{-1} \tag{A.18}$$

$$\boldsymbol{C}_{B_p E_p} = \boldsymbol{q}_{pn}\boldsymbol{C}_{nn}^{-1}\boldsymbol{e}_{pn}^{T} + \boldsymbol{\eta}_{pp} \tag{A.19}$$

$$\boldsymbol{C}_{B_p H_p} = \boldsymbol{q}_{pn}\boldsymbol{C}_{nn}^{-1}\boldsymbol{q}_{pn}^{T} + \boldsymbol{\mu}_{pp} \tag{A.20}$$

$$\boldsymbol{C}_{B_n\varepsilon} = -\left(\boldsymbol{q}_{nn}\boldsymbol{C}_{nn}^{-1}\boldsymbol{C}_{np} - \boldsymbol{q}_{np}\right) \tag{A.21}$$

$$\boldsymbol{C}_{B_n\tau} = \boldsymbol{q}_{nn}\boldsymbol{C}_{nn}^{-1} \tag{A.22}$$

$$\boldsymbol{C}_{B_n E_n} = \boldsymbol{q}_{nn}\boldsymbol{C}_{nn}^{-1}\boldsymbol{e}_{nn}^{T} + \boldsymbol{\eta}_{nn} \tag{A.23}$$

$$\boldsymbol{C}_{B_n H_n} = \boldsymbol{q}_{nn}\boldsymbol{C}_{nn}^{-1}\boldsymbol{q}_{nn}^{T} + \boldsymbol{\mu}_{nn} \tag{A.24}$$

Appendix B. Effective MEE layer characteristics

The MEE layer effective characteristic matrices involved in Eq.(27) and (28) are defined as

$$\begin{aligned}{}^{\varepsilon}_{\delta\varepsilon}\boldsymbol{Q}^{\langle ki\rangle}_{\alpha\beta} = \int_{h_{k-1}}^{h_k} \Big[F^{\langle k\rangle}_{\alpha} F^{\langle k\rangle}_{\beta} \delta_{ik} \Big(\boldsymbol{C}^{\langle k\rangle}_{\sigma\varepsilon} - \boldsymbol{C}^{\langle k\rangle}_{\sigma E_n} \boldsymbol{\mathcal{A}}^{\langle k\rangle}_{\Phi\varepsilon} - \boldsymbol{C}^{\langle k\rangle}_{\sigma H_n} \boldsymbol{\mathcal{A}}^{\langle k\rangle}_{\Psi\varepsilon} \Big) - \\ F^{\langle k\rangle}_{\alpha} \boldsymbol{C}^{\langle k\rangle}_{\sigma E_n} \boldsymbol{a}^{\langle ki\rangle}_{\Phi_\varepsilon\beta} - F^{\langle k\rangle}_{\alpha} \boldsymbol{C}^{\langle k\rangle}_{\sigma H_n} \boldsymbol{a}^{\langle ki\rangle}_{\Psi_\varepsilon\beta} \Big] dx_3\end{aligned} \tag{B.1}$$

$$\begin{aligned}{}^{\tau}_{\delta\varepsilon}\boldsymbol{Q}^{\langle ki\rangle}_{\alpha\mu} = \int_{h_{k-1}}^{h_k} \Big[F^{\langle k\rangle}_{\alpha} \tilde{F}^{\langle k\rangle}_{\mu} \delta_{ik} \Big(\boldsymbol{C}^{\langle k\rangle}_{\sigma\tau} - \boldsymbol{C}^{\langle k\rangle}_{\sigma E_n} \boldsymbol{\mathcal{A}}^{\langle k\rangle}_{\Phi\tau} - \boldsymbol{C}^{\langle k\rangle}_{\sigma H_n} \boldsymbol{\mathcal{A}}^{\langle k\rangle}_{\Psi\tau} \Big) - \\ F^{\langle k\rangle}_{\alpha} \boldsymbol{C}^{\langle k\rangle}_{\sigma E_n} \boldsymbol{a}^{\langle ki\rangle}_{\Phi_\tau\mu} - F^{\langle k\rangle}_{\alpha} \boldsymbol{C}^{\langle k\rangle}_{\sigma H_n} \boldsymbol{a}^{\langle ki\rangle}_{\Psi_\tau\mu} \Big] dx_3\end{aligned} \tag{B.2}$$

$${}^{\xi}_{\delta\varepsilon}\boldsymbol{Q}^{\langle k\rangle}_{\alpha} = -\int_{h_{k-1}}^{h_k} F^{\langle k\rangle}_{\alpha} \Big[\boldsymbol{C}^{\langle k\rangle}_{\sigma E_n} \boldsymbol{a}^{\langle k\rangle}_{\Phi\xi} + \boldsymbol{C}^{\langle k\rangle}_{\sigma H_n} \boldsymbol{a}^{\langle k\rangle}_{\Psi\xi} \Big] dx_3 \tag{B.3}$$

$${}^{\tau}_{\delta\gamma}\boldsymbol{Q}^{\langle ki\rangle}_{\alpha\mu} = \boldsymbol{\mathcal{D}}_i \int_{h_{k-1}}^{h_k} \Big[F^{\langle k\rangle}_{\alpha} \tilde{F}^{\langle k\rangle}_{\mu} \Big] \delta_{ki} dx_3 \tag{B.4}$$

$${}^{\tau}_{\delta u}\boldsymbol{Q}^{\langle ki\rangle}_{\alpha\mu} = \boldsymbol{\mathcal{D}}_i \int_{h_{k-1}}^{h_k} \Big[\frac{\partial F^{\langle k\rangle}_{\alpha}}{\partial x_3} \tilde{F}^{\langle k\rangle}_{\mu} \Big] \delta_{ki} dx_3 \tag{B.5}$$

$$\begin{aligned}{}^{\varepsilon}_{\delta\tau}\boldsymbol{Q}^{\langle ki\rangle}_{\lambda\beta} = \int_{h_{k-1}}^{h_k} \Big[\tilde{F}^{\langle k\rangle}_{\lambda} F^{\langle k\rangle}_{\beta} \Big(-\boldsymbol{C}^{\langle k\rangle}_{\gamma\varepsilon} + \boldsymbol{C}^{\langle k\rangle}_{\gamma E_n} \boldsymbol{\mathcal{A}}^{\langle k\rangle}_{\Phi\varepsilon} + \boldsymbol{C}^{\langle k\rangle}_{\gamma H_n} \boldsymbol{\mathcal{A}}^{\langle k\rangle}_{\Psi\varepsilon} \Big) \delta_{ki} + \\ \tilde{F}^{\langle k\rangle}_{\lambda} \boldsymbol{C}^{\langle k\rangle}_{\gamma E_n} \boldsymbol{a}^{\langle ki\rangle}_{\Phi_\varepsilon\beta} + \tilde{F}^{\langle k\rangle}_{\lambda} \boldsymbol{C}^{\langle k\rangle}_{\gamma H_n} \boldsymbol{a}^{\langle ki\rangle}_{\Psi_\varepsilon\beta} \Big] dx_3\end{aligned} \tag{B.6}$$

$${}^{\gamma}_{\delta\tau}\boldsymbol{Q}^{\langle ki\rangle}_{\lambda\beta} = \boldsymbol{\mathcal{D}}_i \int_{h_{k-1}}^{h_k} \tilde{F}^{\langle k\rangle}_{\lambda} F^{\langle k\rangle}_{\beta} \delta_{ki} \tag{B.7}$$

$${}^{u}_{\delta\tau}\boldsymbol{Q}^{\langle ki\rangle}_{\lambda\beta} = \boldsymbol{\mathcal{D}}_i \int_{h_{k-1}}^{h_k} \tilde{F}^{\langle k\rangle}_{\lambda} \frac{\partial F^{\langle k\rangle}_{\beta}}{\partial x_3} \delta_{ki} \tag{B.8}$$

$$\begin{aligned}{}^{\tau}_{\delta\tau}\boldsymbol{Q}^{\langle ki\rangle}_{\lambda\mu} = \int_{h_{k-1}}^{h_k} \Big[\tilde{F}^{\langle k\rangle}_{\lambda} F^{\langle k\rangle}_{\mu} \Big(-\boldsymbol{C}^{\langle k\rangle}_{\gamma\tau} + \boldsymbol{C}^{\langle k\rangle}_{\gamma E_n} \boldsymbol{\mathcal{A}}^{\langle k\rangle}_{\Phi\tau} + \boldsymbol{C}^{\langle k\rangle}_{\gamma H_n} \boldsymbol{\mathcal{A}}^{\langle k\rangle}_{\Psi\tau} \Big) \delta_{ki} + \\ \tilde{F}^{\langle k\rangle}_{\lambda} \boldsymbol{C}^{\langle k\rangle}_{\gamma E_n} \boldsymbol{a}^{\langle ki\rangle}_{\Phi_\tau\mu} + \tilde{F}^{\langle k\rangle}_{\lambda} \boldsymbol{C}^{\langle k\rangle}_{\gamma H_n} \boldsymbol{a}^{\langle ki\rangle}_{\Psi_\tau\mu} \Big] dx_3\end{aligned} \tag{B.9}$$

$$
{}^{\frac{\partial \varepsilon}{\partial x_1}}_{\delta\tau}\boldsymbol{Q}^{\langle ki\rangle}_{\lambda\beta} = \boldsymbol{I}_1 \int_{h_{k-1}}^{h_k} \Big[\tilde{F}^{\langle k\rangle}_{\lambda} G^{\langle k\rangle}_{\beta} \left(\boldsymbol{C}^{\langle k\rangle}_{\gamma E_p} \boldsymbol{\mathcal{A}}^{\langle k\rangle}_{\Phi\varepsilon} + \boldsymbol{C}^{\langle k\rangle}_{\gamma H_p} \boldsymbol{\mathcal{A}}^{\langle k\rangle}_{\Psi\varepsilon} \right) \delta_{ki} + \tilde{F}^{\langle k\rangle}_{\lambda} x_3 \left(\boldsymbol{C}^{\langle k\rangle}_{\gamma E_p} \boldsymbol{a}^{\langle ki\rangle}_{\Phi_\varepsilon\beta} + \boldsymbol{C}^{\langle k\rangle}_{\gamma H_p} \boldsymbol{a}^{\langle ki\rangle}_{\Psi_\varepsilon\beta} \right) + \tilde{F}^{\langle k\rangle}_{\lambda} \left(\boldsymbol{C}^{\langle k\rangle}_{\gamma E_p} \boldsymbol{b}^{\langle ki\rangle}_{\Phi_\varepsilon\beta} + \boldsymbol{C}^{\langle k\rangle}_{\gamma H_p} \boldsymbol{b}^{\langle ki\rangle}_{\Psi_\varepsilon\beta} \right) \Big] dx_3 \tag{B.10}
$$

$$
{}^{\frac{\partial \varepsilon}{\partial x_2}}_{\delta\tau}\boldsymbol{Q}^{\langle ki\rangle}_{\lambda\beta} = \boldsymbol{I}_2 \int_{h_{k-1}}^{h_k} \Big[\tilde{F}^{\langle k\rangle}_{\lambda} G^{\langle k\rangle}_{\beta} \left(\boldsymbol{C}^{\langle k\rangle}_{\gamma E_p} \boldsymbol{\mathcal{A}}^{\langle k\rangle}_{\Phi\varepsilon} + \boldsymbol{C}^{\langle k\rangle}_{\gamma H_p} \boldsymbol{\mathcal{A}}^{\langle k\rangle}_{\Psi\varepsilon} \right) \delta_{ki} + \tilde{F}^{\langle k\rangle}_{\lambda} x_3 \left(\boldsymbol{C}^{\langle k\rangle}_{\gamma E_p} \boldsymbol{a}^{\langle ki\rangle}_{\Phi_\varepsilon\beta} + \boldsymbol{C}^{\langle k\rangle}_{\gamma H_p} \boldsymbol{a}^{\langle ki\rangle}_{\Psi_\varepsilon\beta} \right) + \tilde{F}^{\langle k\rangle}_{\lambda} \left(\boldsymbol{C}^{\langle k\rangle}_{\gamma E_p} \boldsymbol{b}^{\langle ki\rangle}_{\Phi_\varepsilon\beta} + \boldsymbol{C}^{\langle k\rangle}_{\gamma H_p} \boldsymbol{b}^{\langle ki\rangle}_{\Psi_\varepsilon\beta} \right) \Big] dx_3 \tag{B.11}
$$

$$
{}^{\frac{\partial \tau}{\partial x_1}}_{\delta\tau}\boldsymbol{Q}^{\langle ki\rangle}_{\lambda\mu} = \boldsymbol{I}_1 \int_{h_{k-1}}^{h_k} \Big[\tilde{F}^{\langle k\rangle}_{\lambda} G^{\langle k\rangle}_{\alpha} \left(\boldsymbol{C}_{\gamma E_p} \boldsymbol{\mathcal{A}}^{\langle k\rangle}_{\Phi\tau} + \boldsymbol{C}_{\gamma H_p} \boldsymbol{\mathcal{A}}^{\langle k\rangle}_{\Psi\tau} \right) \delta_{ki} + \tilde{F}^{\langle k\rangle}_{\lambda} x_3 \left(\boldsymbol{C}_{\gamma E_p} \boldsymbol{a}^{\langle ki\rangle}_{\Phi_\tau\mu} + \boldsymbol{C}_{\gamma H_p} \boldsymbol{a}^{\langle ki\rangle}_{\Psi_\tau\mu} \right) + \tilde{F}^{\langle k\rangle}_{\lambda} \left(\boldsymbol{C}_{\gamma E_p} \boldsymbol{b}^{\langle ki\rangle}_{\Phi_\tau\mu} + \boldsymbol{C}_{\gamma H_p} \boldsymbol{b}^{\langle ki\rangle}_{\Psi_\tau\mu} \right) \Big] dx_3 \tag{B.12}
$$

$$
{}^{\frac{\partial \tau}{\partial x_2}}_{\delta\tau}\boldsymbol{Q}^{\langle ki\rangle}_{\lambda\mu} = \boldsymbol{I}_2 \int_{h_{k-1}}^{h_k} \Big[\tilde{F}^{\langle k\rangle}_{\lambda} G^{\langle k\rangle}_{\mu} \left(\boldsymbol{C}^{\langle k\rangle}_{\gamma E_p} \boldsymbol{\mathcal{A}}^{\langle k\rangle}_{\Phi\tau} + \boldsymbol{C}^{\langle k\rangle}_{\gamma H_p} \boldsymbol{\mathcal{A}}^{\langle k\rangle}_{\Psi\tau} \right) \delta_{ki} + \tilde{F}^{\langle k\rangle}_{\lambda} x_3 \left(\boldsymbol{C}^{\langle k\rangle}_{\gamma E_p} \boldsymbol{a}^{\langle ki\rangle}_{\Phi_\tau\mu} + \boldsymbol{C}^{\langle k\rangle}_{\gamma H_p} \boldsymbol{a}^{\langle ki\rangle}_{\Psi_\tau\mu} \right) + \tilde{F}^{\langle k\rangle}_{\lambda} \left(\boldsymbol{C}^{\langle k\rangle}_{\gamma E_p} \boldsymbol{b}^{\langle ki\rangle}_{\Phi_\tau\mu} + \boldsymbol{C}^{\langle k\rangle}_{\gamma H_p} \boldsymbol{b}^{\langle ki\rangle}_{\Psi_\tau\mu} \right) \Big] dx_3 \tag{B.13}
$$

$$
{}^{\xi}_{\delta\tau}\boldsymbol{Q}^{\langle k\rangle}_{\lambda} = \int_{h_{k-1}}^{h_k} \tilde{F}^{\langle k\rangle}_{\lambda} \left(\boldsymbol{C}^{\langle k\rangle}_{\gamma E_n} \boldsymbol{a}^{\langle k\rangle}_{\Phi\xi} + \boldsymbol{C}^{\langle k\rangle}_{\gamma H_n} \boldsymbol{a}^{\langle k\rangle}_{\Psi\xi} \right) dx_3 \tag{B.14}
$$

$$
{}^{\frac{\partial \xi}{\partial x_1}}_{\delta\tau}\boldsymbol{Q}^{\langle k\rangle}_{\lambda} = \boldsymbol{I}_1 \int_{h_{k-1}}^{h_k} \Big[\tilde{F}^{\langle k\rangle}_{\lambda} x_3 \left(\boldsymbol{C}^{\langle k\rangle}_{\gamma E_p} \boldsymbol{a}^{\langle k\rangle}_{\Phi\xi} + \boldsymbol{C}^{\langle k\rangle}_{\gamma H_p} \boldsymbol{a}^{\langle k\rangle}_{\Psi\xi} \right) + \tilde{F}^{\langle k\rangle}_{\lambda} \left(\boldsymbol{C}^{\langle k\rangle}_{\gamma E_p} \boldsymbol{b}^{\langle k\rangle}_{\Phi\xi} + \boldsymbol{C}^{\langle k\rangle}_{\gamma H_p} \boldsymbol{b}^{\langle k\rangle}_{\Psi\xi} \right) \Big] dx_3 \tag{B.15}
$$

$$
{}^{\frac{\partial \xi}{\partial x_2}}_{\delta\tau}\boldsymbol{Q}^{\langle k\rangle}_{\lambda} = \boldsymbol{I}_2 \int_{h_{k-1}}^{h_k} \Big[\tilde{F}^{\langle k\rangle}_{\lambda} x_3 \left(\boldsymbol{C}^{\langle k\rangle}_{\gamma E_p} \boldsymbol{a}^{\langle k\rangle}_{\Phi\xi} + \boldsymbol{C}^{\langle k\rangle}_{\gamma H_p} \boldsymbol{a}^{\langle k\rangle}_{\Psi\xi} \right) + \tilde{F}^{\langle k\rangle}_{\lambda} \left(\boldsymbol{C}^{\langle k\rangle}_{\gamma E_p} \boldsymbol{b}^{\langle k\rangle}_{\Phi\xi} + \boldsymbol{C}^{\langle k\rangle}_{\gamma H_p} \boldsymbol{b}^{\langle k\rangle}_{\Psi\xi} \right) \Big] dx_3 \tag{B.16}
$$

$$
\boldsymbol{J}^{\langle k\rangle}_{\alpha\beta} = \int_{h_{k-1}}^{h_k} \rho^{\langle k\rangle} F^{\langle k\rangle}_{\alpha} F^{\langle k\rangle}_{\beta} dx_3 \tag{B.17}
$$

where δ_{ki} denote the Kronecker delta. It is remarked that the generic effective characteristic matrix ${}^{s}_{r}\boldsymbol{Q}^{\langle pq \rangle}_{\omega\varsigma}$ accounts for the cross-work between the expansion term ς of the field s within the layer q and the expansion term ω of the field r within the layer p; on the other hand, the electric-magnetic effective loading ${}^{s}_{r}\boldsymbol{Q}^{\langle p \rangle}_{\omega}$ accounts for the contribution of the electric-magnetic loading field s within the layer p to the work associated with the variation of the term ω of the field r within the layer p itself.

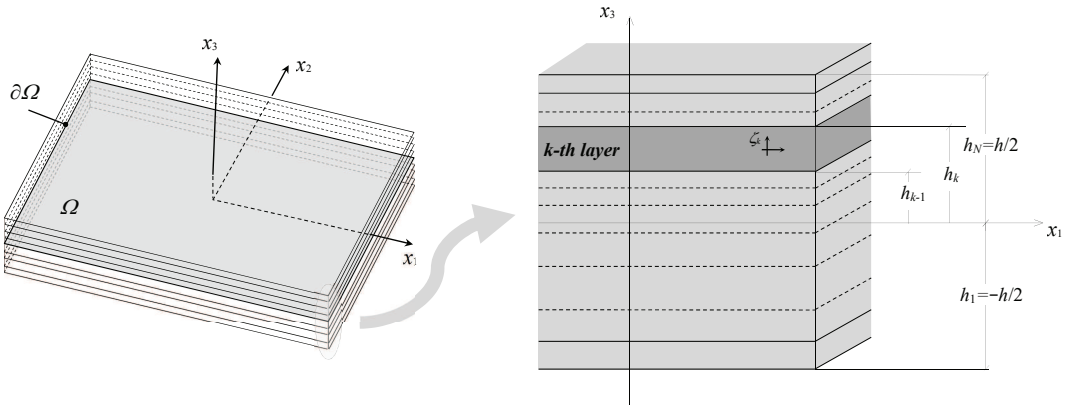

Figure 1: Plate geometrical scheme.

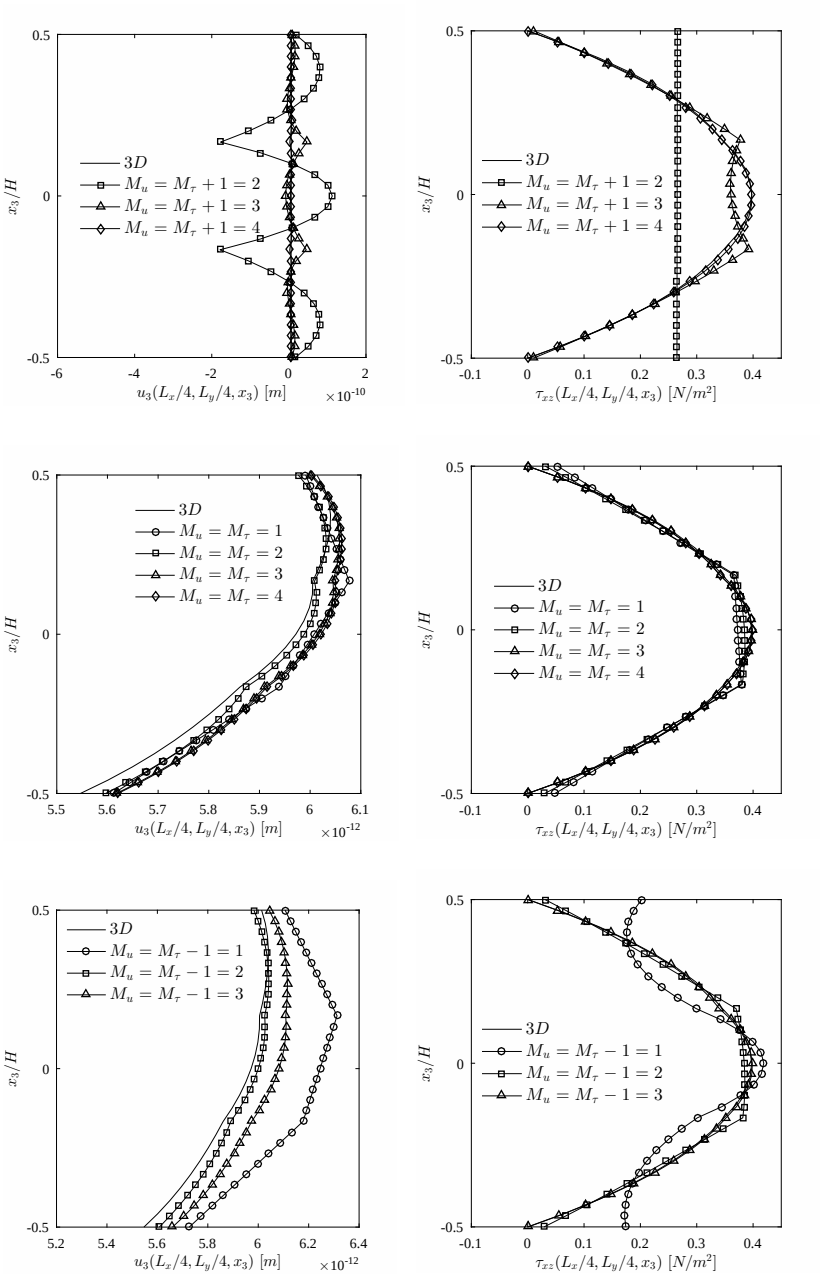

Figure 2: $B/F/B$ simply-supported square plate with $H/L_x = 0.3$ loaded by bi-sinusoidal pressure: through-the thickness distributions at $x_1 = x_2 = 0.25L_x$ for layer-wise models with different variable approximation schemes, namely $M_u > M_\tau$, $M_u = M_\tau$ and $M_u < M_\tau$.

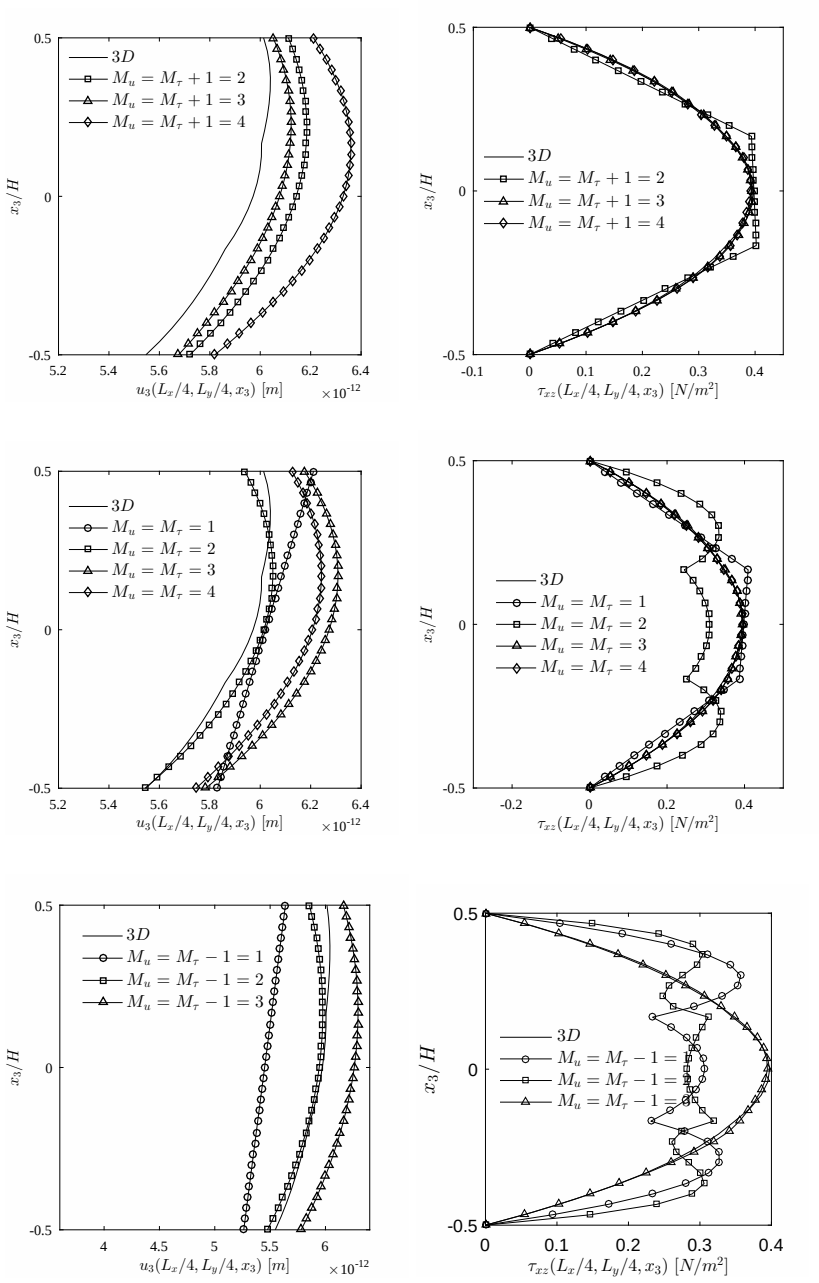

Figure 3: $B/F/B$ simply-supported square plate with $H/L_x = 0.3$ loaded by bi-sinusoidal pressure: through-the thickness distributions at $x_1 = x_2 = 0.25L_x$ for equivalent-single-layer models with different variable approximation schemes, namely $M_u > M_\tau$, $M_u = M_\tau$ and $M_u < M_\tau$.

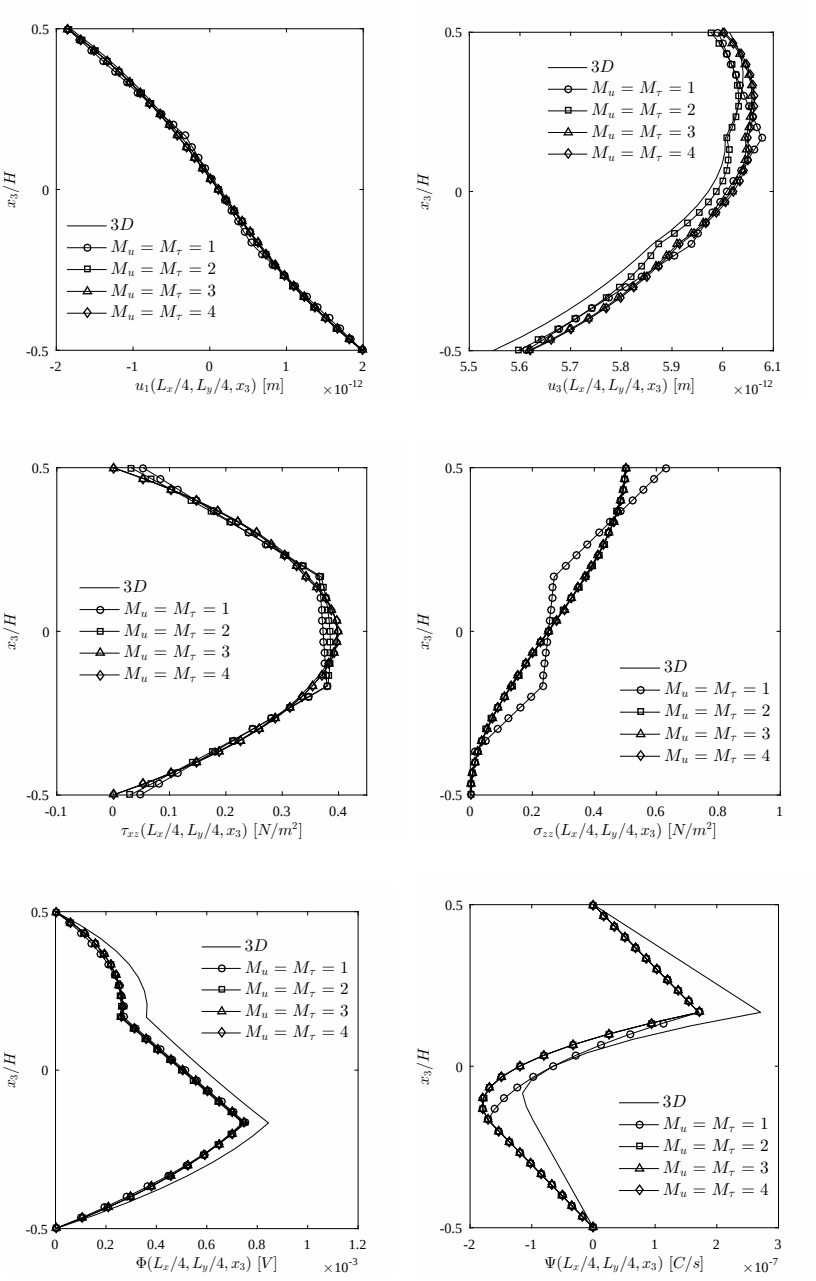

Figure 4: $B/F/B$ simply-supported square plate with $H/L_x = 0.3$ loaded by bi-sinusoidal pressure: through-the thickness distributions at $x_1 = x_2 = 0.25L_x$ for different layer-wise models.

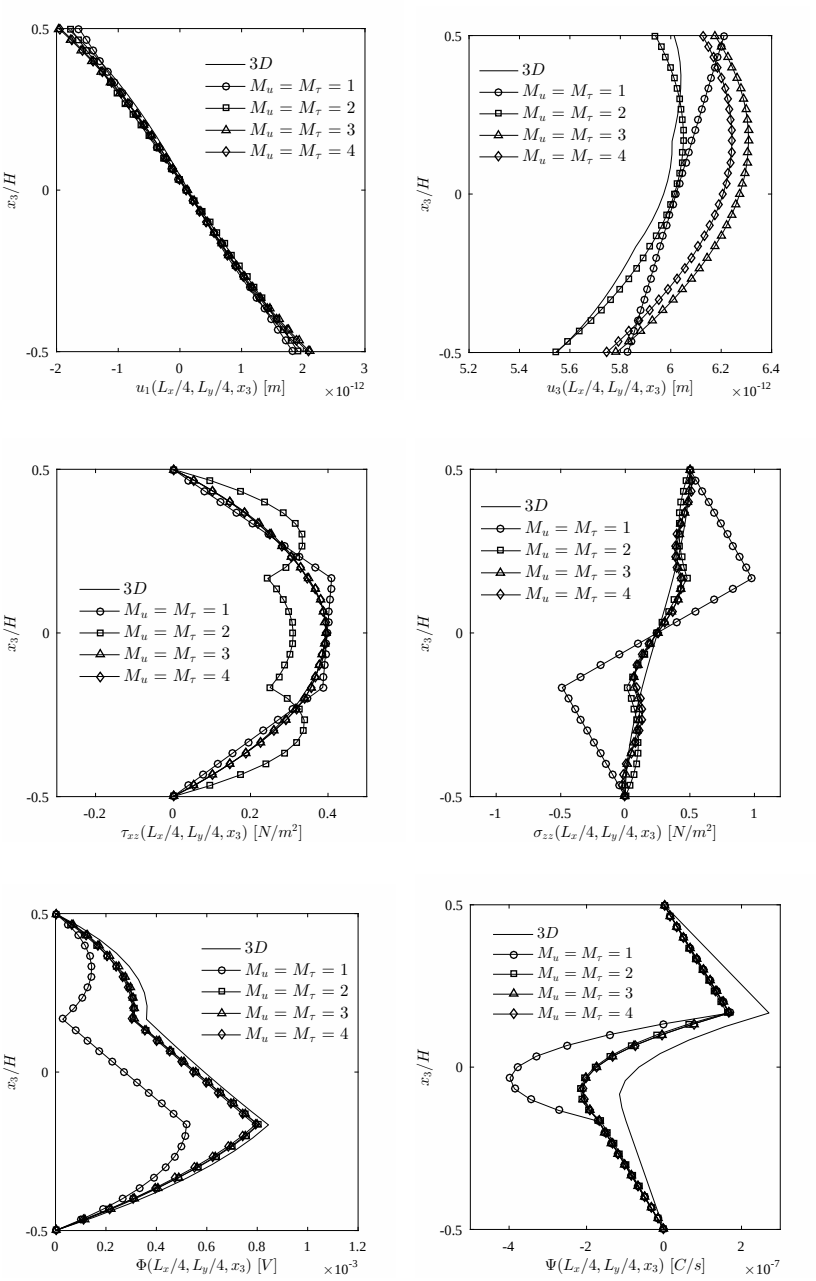

Figure 5: $B/F/B$ simply-supported square plate with $H/L_x = 0.3$ loaded by bi-sinusoidal pressure: through-the thickness distributions at $x_1 = x_2 = 0.25L_x$ for different equivalent-single-layer models.

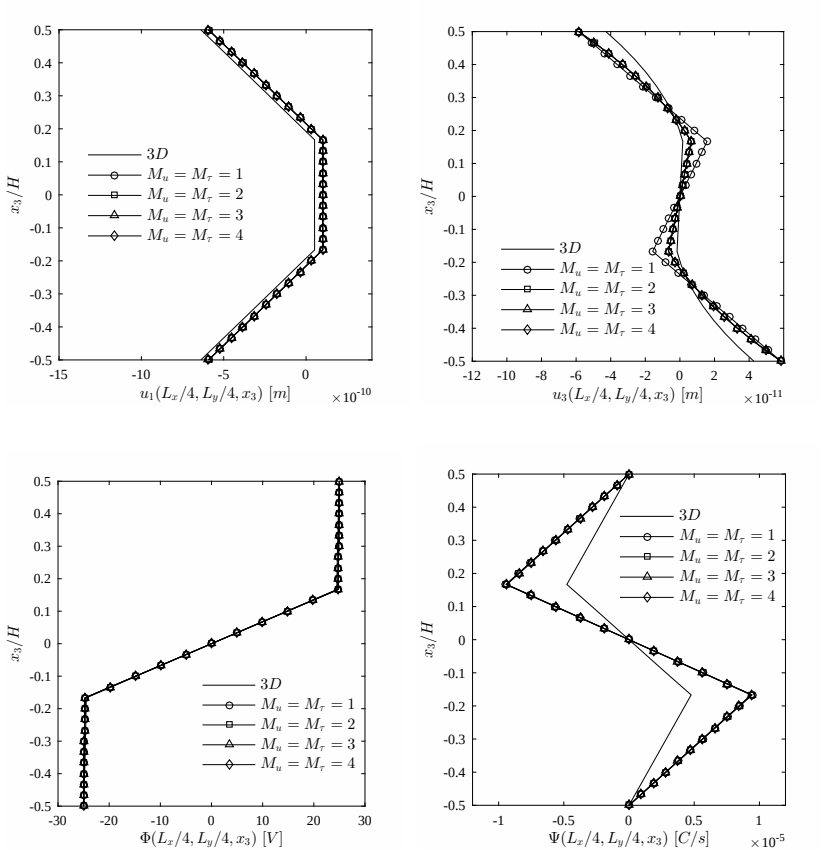

Figure 6: $B/F/B$ simply-supported square plate with $H/L_x = 0.1$ loaded by bi-sinusoidal electric potential: through-the thickness distributions at $x_1 = x_2 = 0.25L_x$ for different layer-wise models.

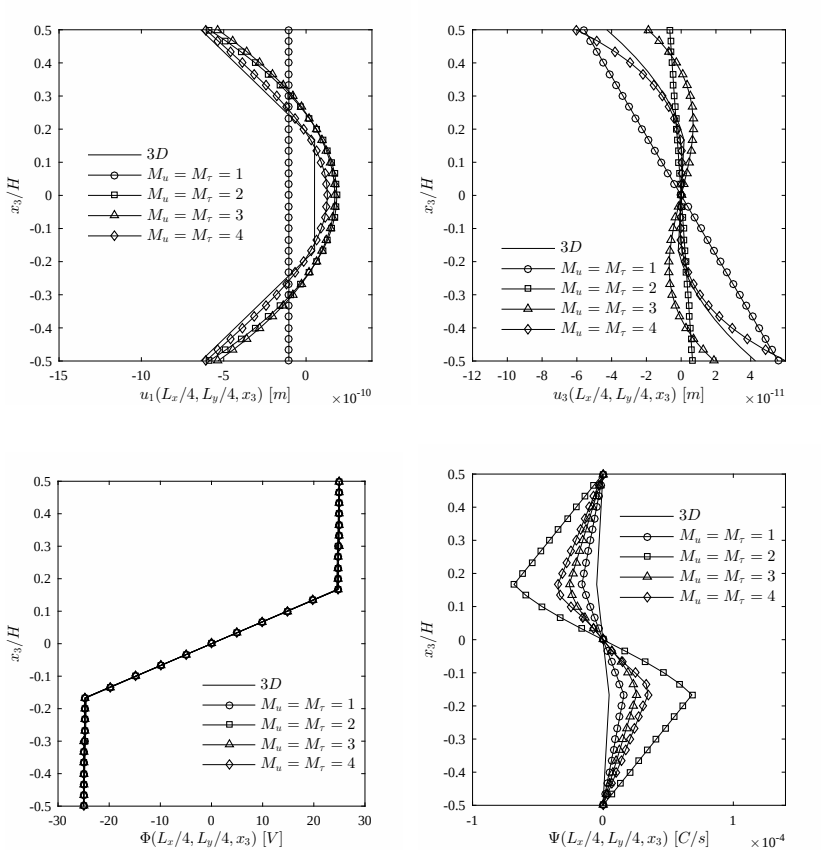

Figure 7: $B/F/B$ simply-supported square plate with $H/L_x = 0.1$ loaded by bi-sinusoidal electric potential: through-the thickness distributions at $x_1 = x_2 = 0.25L_x$ for different equivalent-single-layer models.

	$H/L_x = 0.1$					$H/L_x = 0.3$				
Mode n.	1	2	3	4	5	1	2	3	4	5
$ESL1$	0.406	1.885	3.431	12.874	13.256	0.972	1.885	3.396	4.628	5.534
$ESL2$	0.393	1.885	3.391	13.716	14.030	0.973	1.884	3.335	4.890	5.634
$ESL3$	0.393	1.885	3.276	13.042	13.400	0.956	1.884	3.232	4.681	5.538
$ESL4$	0.391	1.885	3.397	13.043	13.358	0.961	1.884	3.349	4.682	5.424
$LW1$	0.400	1.885	3.432	12.862	13.205	0.976	1.884	3.401	4.628	5.439
$LW2$	0.399	1.885	3.431	13.052	13.378	0.975	1.884	3.399	4.684	5.447
$LW3$	0.399	1.885	3.430	13.042	13.373	0.973	1.884	3.389	4.681	5.455
$LW4$	0.399	1.885	3.430	13.042	13.374	0.973	1.884	3.389	4.681	5.459
$3D$	0.395	1.858	3.294	12.528	13.248	0.961	1.856	3.228	4.497	5.215

Table 1: Normalized natural circular frequencies $\bar{\omega}$ for the $B/F/B$ simply-supported square plate.

	$H/L_x = 0.1$					$H/L_x = 0.3$				
Mode n.	1	2	3	4	5	1	2	3	4	5
$ESL1$	0.474	1.932	3.468	12.316	12.846	1.065	1.932	3.421	4.506	5.721
$ESL2$	0.437	1.932	3.529	13.292	13.682	1.042	1.931	3.451	4.804	5.708
$ESL3$	0.436	1.932	3.488	12.499	12.880	1.030	1.931	3.431	4.561	5.431
$ESL4$	0.435	1.932	3.488	12.500	12.878	1.027	1.931	3.429	4.561	5.419
$LW1$	0.439	1.932	3.467	12.361	12.733	1.040	1.931	3.407	4.517	5.363
$LW2$	0.435	1.932	3.467	12.500	12.878	1.027	1.931	3.406	4.561	5.418
$LW3$	0.435	1.932	3.467	12.492	12.870	1.027	1.931	3.407	4.558	5.416
$LW4$	0.435	1.932	3.467	12.492	12.870	1.027	1.931	3.407	4.558	5.416
$3D$	0.444	1.960	3.478	12.997	13.961	1.067	1.960	3.388	4.742	5.895

Table 2: Normalized natural circular frequencies $\bar{\omega}$ for the $F/B/F$ simply-supported square plate.